Picosecond real-time studies of mode-specific vibrational predissociation

David H. Semmes, J. Spencer Baskin, and Ahmed H. Zewail
Arthur Amos Noyes Laboratory of Chemical Physics,[a] *California Institute of Technology, Pasadena, California 91125*

(Received 13 October 1989; accepted 13 November 1989)

The vibrational predissociation of several van der Waals complexes of *t*-stilbene has been studied by directly measuring, in real time, the fluorescence intensity from the initial reactant state and from the individual product states formed in the dissociation process after exciting single vibrational levels of the complex. With the aid of a kinetic model involving sequential processes, the individual rates for intramolecular vibrational redistribution and vibrational predissociation in the overall dissociation process are resolved and distinguished in several cases. In the stilbene–He complex, the dissociation is significantly faster from low energy out-of-plane modes than it is from a higher energy in-plane mode.

I. INTRODUCTION

In the absence of collisions, the yield and rate of unimolecular dissociation will be determined by the specific rate of intramolecular vibrational-energy redistribution (IVR) from the initial mode excited to the other modes in the molecule and by the rate of bond breaking (vibrational predissociation, VP). If k_{IVR} is larger than k_{VP}, then the chemistry may be from a statistically formed distribution of vibrational states and a statistical behavior [Rice–Ramsberger–Kassel–Marcus theory (RRKM)] may prevail, even if a laser is used to selectively excite the initial state of the reagent. It is this interplay between IVR and VP that determines the mode selectivity of the reaction. Excitation of the molecule with short enough pulses, short compared to k_{IVR}^{-1} and k_{VP}^{-1}, should allow us to view these processes in real time and hopefully establish conditions for nonstatistical behavior.

In an earlier communication,[1] we reported observation of mode-selective photofragmentation dynamics for the system

$$\text{stilbene–He} \rightarrow \text{stilbene} + \text{He}.$$

Real-time measurements of the reaction rates of the van der Waals molecule stilbene–He were given as a function of reagent and product internal energies. The results showed a mode-dependent, rather than energy-dependent, unimolecular decay rate and a mode dependence in the rate of product formation up to an excess vibrational energy of four times the bond energy. Here, we extend the study on the mode specificity of the dissociation to three higher combinations of the stilbene–He bands. The dissociation from the fundamental and overtones of a single mode in stilbene–He_2, –Ne, and –Ar is also reported. We provide analysis of the IVR process, the predissociation rates, and compare the results with available theories.

The stilbene system is attractive to study for a number of reasons. The excitation spectrum of *trans*-stilbene[2] and its van der Waals complexes[3] have been published. The excitation spectrum of the helium complex shows a vibrational mode-selective line broadening.[3(b),3(c)] Furthermore, the IVR dynamics of stilbene have been thoroughly characterized.[4] The stoichiometry (1:1 or 1:2) and the geometry of the complexes have been determined by sub-Doppler measurements of the rotational constants of the emitting species.[5] Finally, recent spectroscopic studies by the groups of Ito[6] and Zwier[7] have provided valuable information that is relevant to the present study.

This paper is outlined as follows: Sec. II includes a discussion of the experimental method and analysis of the kinetic information that is available from temporal data. In Sec. III the results from each excitation we have studied are reported. Section IV examines the results and compares them with theoretical expectations. We conclude in Sec. V.

II. EXPERIMENTAL

A. Apparatus

Stilbene–rare gas complexes were formed in continuous supersonic jet expansions into a vacuum chamber held at less than 1 mTorr. To produce stilbene–neon and stilbene–argon complexes, approximately 100 psi of a mixture of a small percentage of neon or argon in helium was passed over stilbene heated to ~125 °C in a Pyrex tube and expanded through a 50–80 μ pinhole. To form a sufficient concentration of stilbene–helium, it was necessary to increase the backing pressure to as high as 800 psi of helium and to use a stainless steel high pressure nozzle assembly with a 25 μ pinhole.

The complexes formed in these expansions were excited with tunable UV pulses of light ~ 15 ps [full width at half-maximum (FWHM)] long and ~2 cm^{-1} (FWHM) broad. These pulses were the doubled output of a cavity-dumped dye laser (R6G in ethylene glycol) synchronously pumped by a mode-locked Ar^+ laser.

The laser-induced fluorescence from the sample in the jet expansion was focused onto the slit of a 1/2 m monochromator, detected and time resolved by either a Hammamatsu R1564U or R2287U microchannel plate photomultiplier tube with associated photon counting electronics. The system response function measured with the Hammamatsu R2287U was generally broader, but more stable in position and width than that of the R1564U. The temporal system response function was measured by moving the molecular beam nozzle assembly into the path of the laser beam and detecting the scattered light. The response function for the

[a] Contribution No. 8054.

 0021-9606/90/063359-18$03.00

R2287U usually had a full width at half maximum of about 80 ps.

This apparatus, except for the high pressure nozzle assembly, has been described in detail before.[8]

B. Analysis

Data is fit to the most simple exponential form possible. The method of nonlinear least-squares curve fitting[9] was used with Marquardt's algorithm[9] to fit the experimental data to single, double, and triple exponential forms convoluted with the measured system response function. That is, the data is fit as the sum of one, two, or three exponential components with independent amplitudes which may be positive or negative in sign. Negative amplitudes reflect rise times and positive amplitudes reflect decay times. The residual of the fit (i.e., the number of standard deviations each point is away from the fit) was calculated and plotted. Values of the reduced χ^2 statistic (χ_r^2) for all our reported data are less than 1.10. Our evidence for the validity of the fit is based on two practical observations. First, in the fluorescence of the resonantly excited bare aromatic molecule, we have a "standard" single exponential with which we can compare other temporal data. Secondly, we will show that our data were collected to a high enough signal-to-noise that data which have additional, fast components can be distinguished from data that do not.

The convoluted rise in any measured temporal data depends sensitively on the width, shape, and position of the system response function and also contains most of the signal due to fast rising or decaying lifetime components. Therefore, for this work it was important to measure the correct response, i.e., the response that corresponds to the measured temporal data, and also for the response to remain stable during the measurement of a decay curve.

Most critical is the precise way in which laser light is scattered to measure the system response function and the signal is focused onto the photomultiplier to measure the temporal data. In preliminary experiments, when changing only the alignment of the molecular beam and the collection optics, we observed a shift in the peak of the response as large as $\sim 2/3$ of the full width at half maximum (FWHM). This shift is likely due to transit time effects from detecting the light scattered onto different parts of the microchannel plate photomultiplier tube (PMT) cathode. Before we could consistently and accurately measure the rising part of the temporal data, convoluted with the system response function, it was necessary to align the molecular beam and detection optics so that an accurate response, not shifted with respect to the temporal data or distorted in shape, could be consistently measured.

In addition, it was necessary to discriminate against rotational coherence effects[5] in order to accurately measure the convoluted rises of temporal data. To accomplish this for the signal-to-noise levels of the data in this work, it was sufficient to align the plane of the laser polarization so that equal amounts of parallel and perpendicular fluorescence were detected. It was not necessary to detect fluorescence at the magic angle (and thus lose signal from having to introduce a polarizer into the collection optics.) Finally, it was necessary to keep the temperature of the stilbene in the molecular beam reservoir near or below the melting point of stilbene. At higher temperatures resonantly excited stilbene fluorescence appeared to have a fast (~ 20 ps) rising component.

Taking these problems into consideration, single exponential decays of resonantly excited fluorescence from the bare molecule could consistently be fit from the sharp, convoluted rise to the end of the decay (see Fig. 1). Such a single exponential decay was collected and fit at the beginning and end of each day as a control experiment. In addition, the system response function was monitored periodically throughout each day so that drifts and changes in its shape were recognized.

Figure 2 shows the difference between single and double exponential fits of the fast rise in the fluorescence from bare, vibrationless stilbene formed after exciting stilbene–He at 95 cm^{-1}. Note the different scales in the residuals of the two fits. Identical response functions of FWHM = 82 ps were measured before and after this data. The single exponential fit is shifted 26 ps with respect to the measured response so that the fit intersects the middle of the measured rise of the data, entirely missing experimental data points before and after. This systematic error also appears clearly in the residual. By contrast, the shift of the double exponential fit in Fig. 2 is <2 ps.

In a similar way, Fig. 3 compares double and triple exponential fits to the temporal data for the fluorescence of vibrationless stilbene formed after exciting stilbene–Ne at 198 cm^{-1}. Identical system response functions were measured directly before and after this data, as were well-fit decays of resonantly excited bare stilbene. Again, the incorrect fit alternately deviates from the experimental data and is shifted from the measured response substantially (32 ps) so as to minimize the effect of the fast lifetime that has not been accounted for. Furthermore, although the eight fit param-

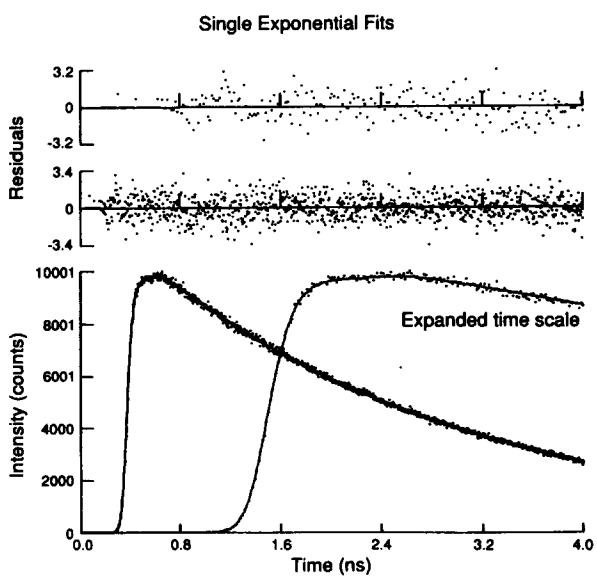

FIG. 1. Fluorescence decay of resonance emission from bare stilbene excited to the vibrational level $36^2 37^2$, fit as a single exponential decay ($\tau_f = 2.6$ *ns*) convoluted with the system response function. The full width at half maximum of the measured system response function Δ was 82 ps. For this fit, $\chi_r^2 = 1.09$.

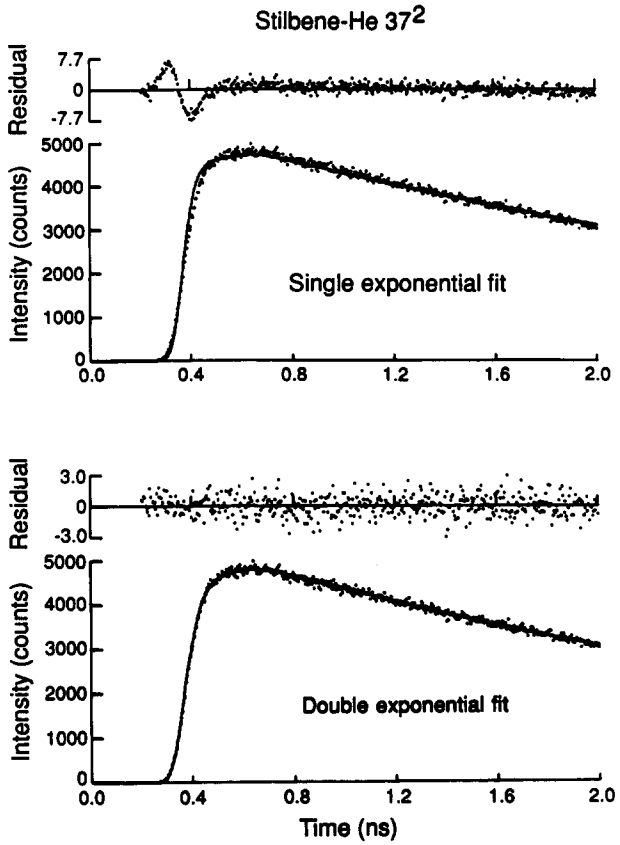

FIG. 2. Single and double exponential fits of the emission from bare, vibrationless stilbene formed in the dissociation of stilbene–He 37^2. $\Delta = 82$ ps and $\chi_r^2 = 3.64$ and 1.04, respectively.

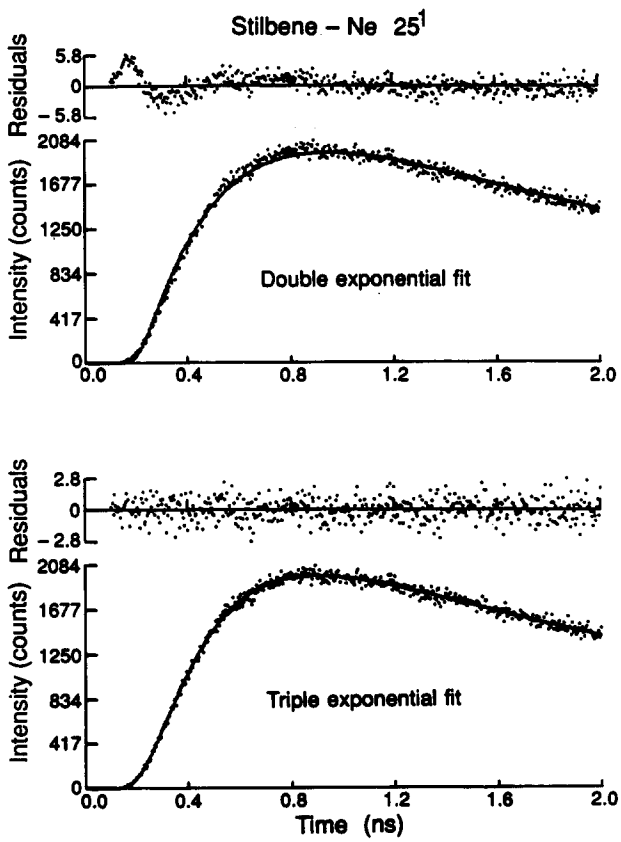

FIG. 3. Double and triple exponential fits of the emission from bare, vibrationless stilbene formed in the dissociation of stilbene–Ne 25^1. $\Delta = 76$ ps and $\chi_r^2 = 1.96$ and 0.93, respectively.

eters of the triexponential were treated as entirely independent, the ratios of the amplitudes of the fast lifetime components to the amplitude of the fluorescent decay, -1.34 and 0.36, are the same within experimental error as those calculated from the lifetimes using a kinetic scheme we will discuss in Sec. IV B.

During the course of the experimental work described in this paper, the two decays plotted in Figs. 2 and 3 were measured, respectively, four and six times, independently, on different days, under different conditions of laser power, total pressure, etc. The standard deviation of each of the measured lifetimes and amplitude ratios for the repeated measurements of those decays were all under 10%. This figure gives the most realistic estimate of the error in the measured lifetimes and amplitudes. In the text, the average of the measured lifetimes will be reported.

Additional estimates of the errors in fitting these curves were obtained by "synthesizing" data with an experimental response function that has been broadened artificially to represent a drifting or abruptly shifting response, and fitting the "synthesized data" with the unchanged response function. While the effect of a continuously drifting response is generally to add an apparent rising component to the data, the data is well fit by the smaller, correct number of exponentials until the shift is $\frac{1}{2}$ to $\frac{3}{4}$ of the FWHM of the response. Experimentally, shifts in the response during the measurement were usually $< \frac{1}{10}$ of the FWHM.

Using such synthesized data and inspecting the residual as above, we conclude that with an 80 ps FWHM response function and collecting about 3000 counts of signal at the maximum of a data curve, we can resolve risetimes in the temporal data as short as ≈ 20 ps.

III. RESULTS

A. Complexes with helium

1. Stilbene–He

Excitation bands corresponding to excited stilbene transitions in the stilbene–He complex have been observed $6 \pm 1\ \text{cm}^{-1}$ to the red of the corresponding bare stilbene transition for each transition of the molecule.[3] Seven of these bands, all overtones and combinations of ν_{25} ($198\ \text{cm}^{-1}$), ν_{36} ($35\ \text{cm}^{-1}$), and ν_{37} ($48\ \text{cm}^{-1}$) have been studied in these experiments.

a. 0_0^0. The fluorescence spectrum of vibrationless S_1 stilbene has been observed[2] and assigned[2,6] as primarily involving progressions of ν_{37} built on each member of a progression in ν_{25}. The frequency of each member in the ν_{37} progressions, however, depends on the transition with which it combines, apparently because of the large anharmonicity of ν_{37}. The stilbene–He origin fluorescence spectrum is very similar. Each member of the ν_{25} progression is shifted $6\ \text{cm}^{-1}$ to the red, just as the complex bands are shifted 6 cm^{-1} to the red in the excitation spectrum. The ν_{37} progressions, however, are shifted between 3 and 6 cm^{-1} to the red and have different intensity distributions.

The fluorescence decay is fit by a single exponential, the lifetime of which is equal to the lifetime of bare stilbene at this energy (2.67 ns).[10] Time-resolved polarization anisot-

ropy experiments identify the emitter as stilbene–He.[5] Thus, exciting the vibrationless level of the complex, no unusual dynamical behavior is observed.

b. 83 and 95 cm^{-1}. The shifts of these complex excitation bands from the corresponding bare stilbene bands are $\sim 1\ \mathrm{cm}^{-1}$ less than the shift of the origin according to Zwier.[3(c)] Although these vibrational frequencies are therefore slightly different in the complex, for simplicity we will use the vibrational frequencies of the bare molecule ($S_1 + 83\ \mathrm{cm}^{-1}$ and $S_1 + 95\ \mathrm{cm}^{-1}$) in referring to the complex levels $36^1 37^1$ and 37^2. These excitation bands are distinguished by their unusual breadth[3(b)] and the tuning dependence of the product yields.[3(c)] Figure 4 shows the fluorescence spectra for excitation at the peaks and 1.5–2 cm^{-1} red and blue of the peaks of those bands. The major product at both excitation bands is vibrationless stilbene and is formed in 42 ps after exciting the complex at 95 cm^{-1} (see again Fig. 2) and in 36 ps after exciting the complex at 83 cm^{-1}, independently of the precise excitation wavelength. In both cases, the minor product is produced by loss of one quantum of ν_{37} and is formed unresolvably fast. The rises in these temporal data are compared with each other in Fig. 5.

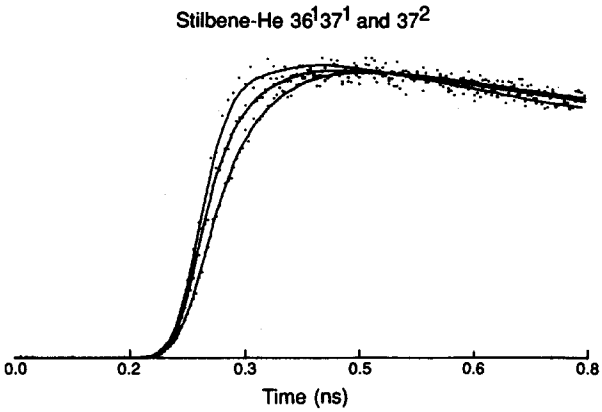

FIG. 5. Rise times in the fluorescence of product in the reactions: stilbene–He $37^2 \rightarrow$ stilbene 37^1 + He, $\tau < 20$ ps; stilbene–He $37^2 \rightarrow$ stilbene 0^0 + He, $\tau = 43$ ps; stilbene–He $36^1 37^1 \rightarrow$ stilbene 0^0 + He, $\tau = 34$ ps. $R = 0.5$ Å and $\Delta = 56$ ps for the 0^0 data. For the 37^1 data, $R = 3.2$ Å and $\Delta = 80$ ps. χ_r^2 equals 1.01, 1.05, and 1.01, respectively, for the three fits.

c. 198 cm^{-1}. The complex 198 cm^{-1} excitation band (25_0^1) overlaps with the bare stilbene $2\times 95\ \mathrm{cm}^{-1}$ band. Dispersed fluorescence spectra recorded under identical conditions except for the backing pressure of the molecular beam are shown in Fig. 6, traces a and b. Trace c is a normalized difference spectrum. Assuming that there are two independent absorbers contributing to this spectrum, all of the bands in this spectrum must be due to the absorber whose relative concentration is higher at higher pressures. Our studies of the pressure dependence of the concentration of the complex and of the bare molecule show that the concentration of the complex increases rapidly with pressure over this pressure range, while the concentration of the bare molecule decreases slightly. This trace is therefore the best experimental approximation to the complex spectrum and the normalization constant is consistent with our pressure dependence studies.

None of the bands in the spectrum of the complex can be assigned to known S_1 states.[1] The fluorescence intensity from various weak bands, including the resonant band at the laser wavelength, decay with a 159 ps lifetime and various stronger bands have that risetime, with no resolvable third component (Fig. 7).

d. 280 and 292 cm^{-1}. These broad[3] absorption bands are assigned as the combinations $198 + 83\ \mathrm{cm}^{-1}$ ($25^1 36^1 37^1$) and $198 + 95\ \mathrm{cm}^{-1}$ ($25^1 37^2$). Both complex bands overlap with bands in bare stilbene. Figure 8 shows the fluorescence spectra of these overlapping bands at 280 cm^{-1} with backing pressures of 600 and 200 psi helium, a normal-

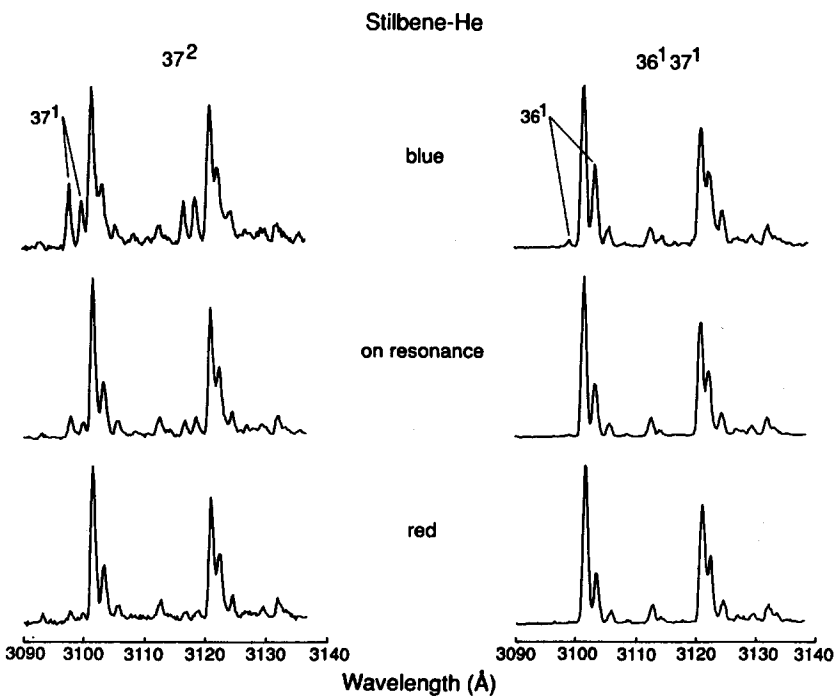

FIG. 4. Dispersed fluorescence spectra (spectral resolution, $R = 0.5$ Å) from exciting the maximum, the red edge, and the blue edge of the broad stilbene–He 37_0^2 and $36_0^1 37_0^1$ excitation bands.

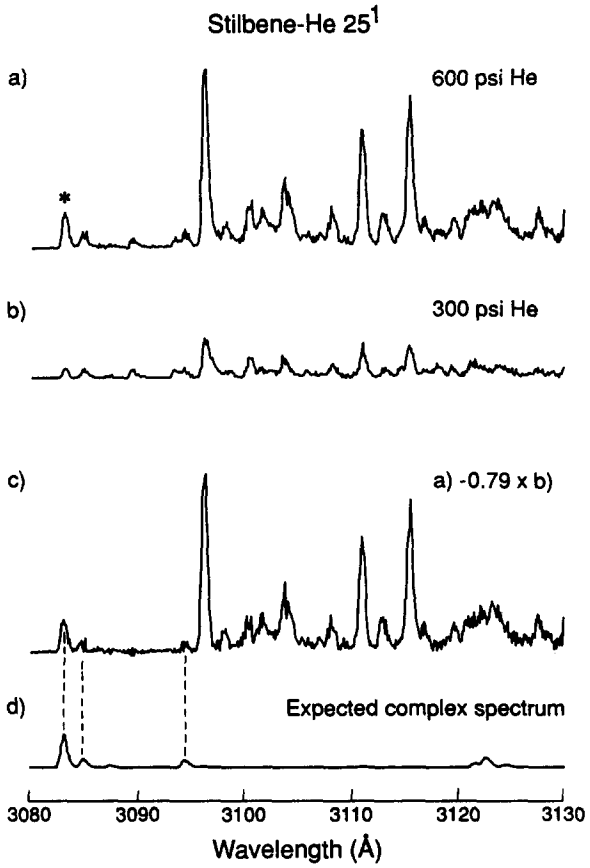

FIG. 6. Dispersed fluorescence spectra ($R = 0.2$ Å) of overlapping emission from stilbene–He 25^1 and stilbene 37^4 with molecular beam backing pressures of 600 and 300 psi helium (traces a and b, respectively). The excitation wavelength is marked in trace a. Trace c, emission due to absorption of the complex, was obtained by subtracting trace b from trace a, normalizing the intensity so that the peak at 3088.9 Å is completely attributed to absorption of bare stilbene. Trace d shows the emission spectrum expected from the complex, i.e., a spectrum identical to that from the bare molecule at 198 cm^{-1}, but shifted 6 cm^{-1} red.

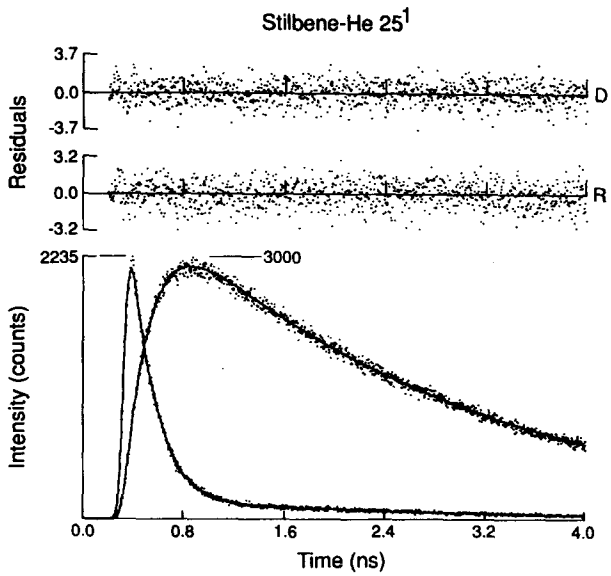

FIG. 7. Temporal data for the decay ($\tau = 160$ ps, $\chi_r^2 = 1.09$) of stilbene–He 25^1 fluorescence at 3094.8 Å and the rise ($\tau = 173$ ps, $\chi_r^2 = 1.10$) in the fluorescence ($\lambda = 3096.4$ Å) of the stilbene formed. $R = 0.3$ and 0.2 Å, respectively, and $\Delta = 82$ ps. The data for the decay of stilbene–He is fit with an additional 2.3 ns decay with an amplitude smaller by a factor of 20. At the excitation wavelength, the amplitude of the long component is smaller by a factor of about 100. The residual identified by a "D" is for the data with a fast decaying component and the residual identified by an "R" is for the data with a fast rising component.

ized difference spectrum, and a spectrum of bare stilbene at 198 cm^{-1}. It is evident that the emission due to absorption of the complex is from bare stilbene in the 198 cm^{-1} state. From the complex excited to 280 cm^{-1}, that single product is formed in ~18 ps. As discussed in the previous section, the limit of the temporal resolution is ~20 ps. Figure 9 compares the residuals for the single exponential best fit and for the double exponential best fit for this data. Since no systematic error was observed in the convoluted rise of the fluorescent decays of resonantly excited bare stilbene when these data were measured, this is evidence for a fast rise in the fluorescence decay of the stilbene[1] formed. The vibrational product state distribution from the complex excited to 292 cm^{-1} depends on the precise excitation wavelength, as at 95 cm^{-1}. Product formed by the loss of a single quantum of ν_{37} ($25^1 37^1$) is formed unresolvably fast, while stilbene at 198 cm^{-1} is formed in ~22 ps.

e. 396 cm^{-1}. The complex 25_0^2 excitation band overlaps with the bare stilbene $25_0^1 37_0^4$ band (Fig. 10). As at 198 cm^{-1}, the emission bands due to the complex cannot be assigned to known complex or stilbene bands. The resonant complex fluorescence decays in 58 ps and several of the more intense complex lines have the same rise time with no apparent third component (Fig. 11).

2. Stilbene–He_2

Bands in the excitation spectrum of stilbene–He_2 have been identified[3] 12 cm^{-1} to the red of the corresponding stilbene transitions at the origin and the fundamental and overtones of ν_{25}. Such transitions have not been observed for stilbene transitions in the complex corresponding to combinations and overtones of ν_{36} and ν_{37}. The only stilbene–He_2 excitations studied are at 198 cm^{-1}, the stilbene ν_{25} band, and 396 cm^{-1}, its overtone.

a. 198 cm^{-1}. The fluorescence spectrum of stilbene–He_2 at 198 cm^{-1}, not complicated by overlapping absorptions, is shown in Fig. 12. Bands assigned to the major product, vibrationless stilbene, and the minor products 36^1 and 37^1 stilbene are indicated in the figure along with the band due to resonant emission. A 90 ps decay of the initially excited state was measured, as was a well fit triexponential decay of the stilbene origin fluorescence (Fig. 13). The triexponential included a decaying component with a 42 ps lifetime in addition to the 2.7 ns fluorescence decay and 94 ps rise time, with the amplitudes of the three components related to the measured lifetimes as will be discussed in Sec. IV B. However, this decay was equally well fit (as judged by the value of χ_r^2) as a biexponential with a 115 ps rise time, but a 30 ps shift with respect to the measured response. A similar shift was found when triexponentials with those parameters were simulated and fit as biexponentials.

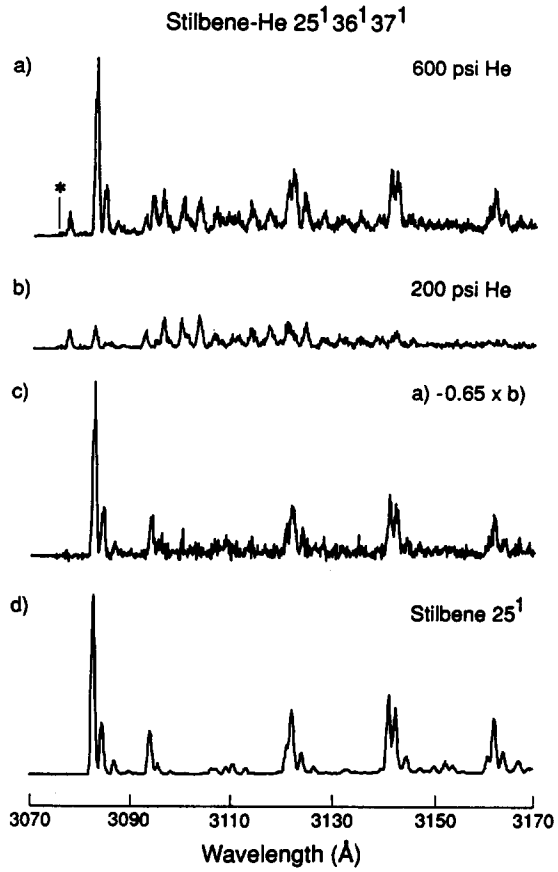

FIG. 8. Dispersed fluorescence spectra ($R = 0.5$ Å) of overlapping emission from stilbene–He $25^1 36^1 37^1$ and stilbene $36^1 37^5$ with molecular beam backing pressures of 600 and 200 psi helium (traces a and b, respectively). The excitation wavelength is marked in trace a. Trace c, emission due to absorption of the complex, was obtained by subtracting trace b from trace a, normalizing the intensity so that the bluest major peak is completely attributed to absorption of bare stilbene. The spectrum of stilbene 25^1 (trace d) is also shown for comparison.

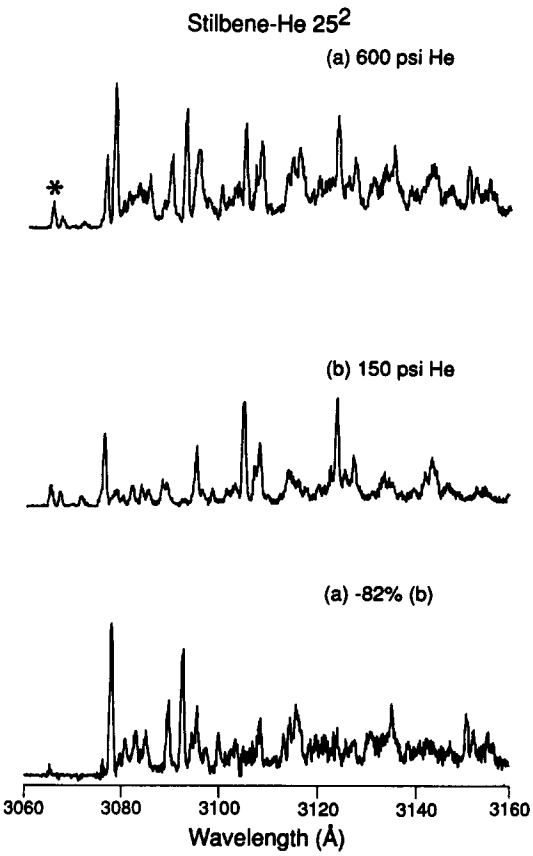

FIG. 10. Dispersed fluorescence spectra ($R = 0.5$ Å) of overlapping emission from stilbene–He 25^2 and stilbene $25^1 37^4$ and the normalized difference spectrum.

The measured decay of fluorescence from the state 37^1 depends markedly on the spectral resolution, presumably because of underlying complex emission. At high resolution ($8\ \mathrm{cm}^{-1}$), a low signal-to-noise measurement of the time-

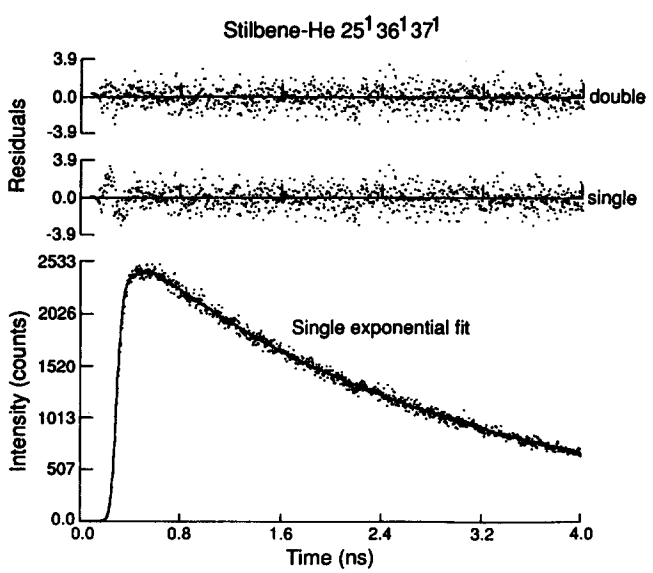

FIG. 9. Rise time in the fluorescence of product in the reaction: stilbene–He $25^1 36^1 37^1 \rightarrow$ stilbene 25^1 + He. $R = 0.8$ Å and $\Delta = 90$ ps. The best fit is a biexponential with an 18 ps rise time, with $\chi_r^2 = 1.08$. The best single exponential fit (shown) rises slightly faster than the data.

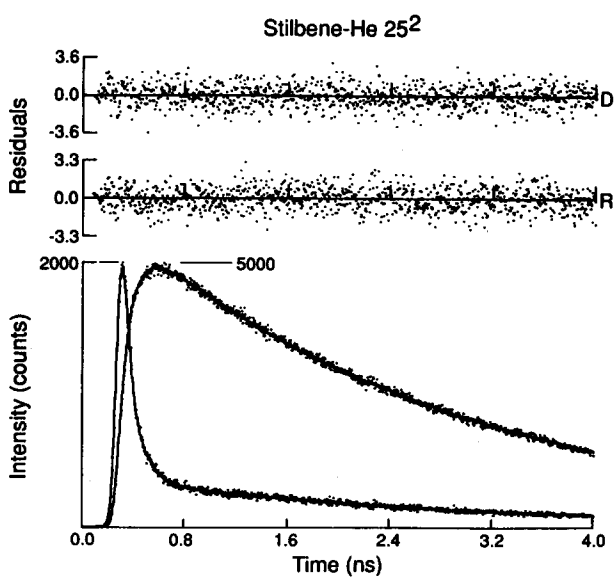

FIG. 11. Temporal data for the decay ($\tau = 60$ ps, $\chi_r^2 = 1.01$) of stilbene–He 25^2 fluorescence at 3064.3 Å and the rise ($\tau = 56$ ps, $\chi_r^2 = 0.97$) in the fluorescence ($\lambda = 3077.2$ Å) of the stilbene formed. $R = 0.8$ Å and $\Delta = 84$ ps. The pressure in the molecular beam was 600 psi. The long component in the data for the fast decay is unchanged at low backing pressure.

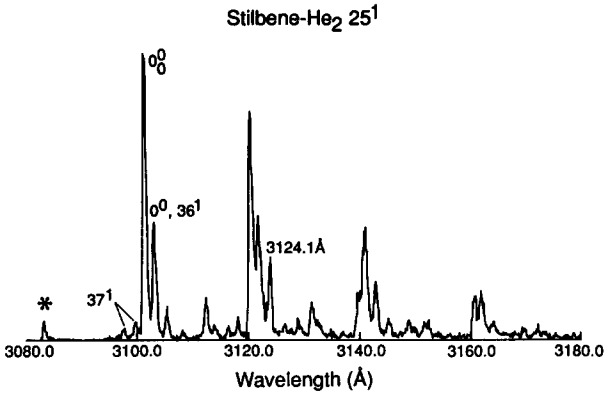

FIG. 12. Dispersed fluorescence spectrum ($R = 0.5$ Å) of stilbene–He_2 25^1. The band at 3124.1 Å has not been assigned.

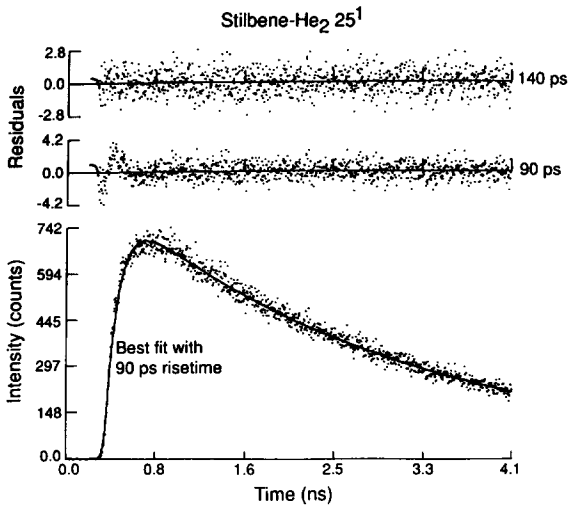

FIG. 14. Temporal data for the product of the reaction: stilbene–He_2 25^1 $\rightarrow$stilbene 37^1 + 2He fit with a 90 ps rise, $\chi_r^2 = 1.12$. The best fit, with $\tau = 140$ ps, has $\chi_r^2 = 0.92$. $R = 0.8$ Å and $\Delta = 84$ ps.

resolved fluorescence from this level is best fit with a partial rise time (the ratio of the amplitude of the two components is ~ -0.4 rather than -1.0) of 140 ps. Figure 14 shows this data and the residuals of the best biexponential fit with a 90 ps rise time and the best biexponential fit.

b. 396 cm^{-1}. The fluorescence spectrum of stilbene–He_2 excited to 25_0^2, again not complicated by overlapping bands, is shown in Fig. 15. Most of the fluorescence is from stilbene excited with one quantum of ν_{25} [cf. Fig. 8(d)]. The fluorescence of this product rises with the same rate as the decay rate of the resonant fluorescence 1/(34 ps) with no detectable third component in the temporal profile (see the data with fast decay and fast rise in Fig. 16). Vibrationless stilbene and stilbene 25^137^1 are recognized as minor products, and bands assigned to these levels are labeled in the figure. These bands overlie a background of unidentified product and complex emission. The vibrationless stilbene product was previously reported and a decay measured at 3101.4 Å was fit as a biexponential with a 118 ps rise time.[1] We have repeated this measurement to a signal-to-noise more than three times larger and have fit the data, not as a biexponential, but as a triexponential with rising components of both 48 and 243 ps (see data labeled "slower rise" in Fig. 16). While it is doubtful that we have accurately resolved the time evolution of the vibrationless product due to the low intensity of its emission and the congestion of the fluorescence spectrum, details of the dynamics leading to origin stilbene can still be deduced from the presence of the strong, long rise time. (Emission from the product 25^137^1 is far too weak to accurately measure the time evolution of formation for that state.)

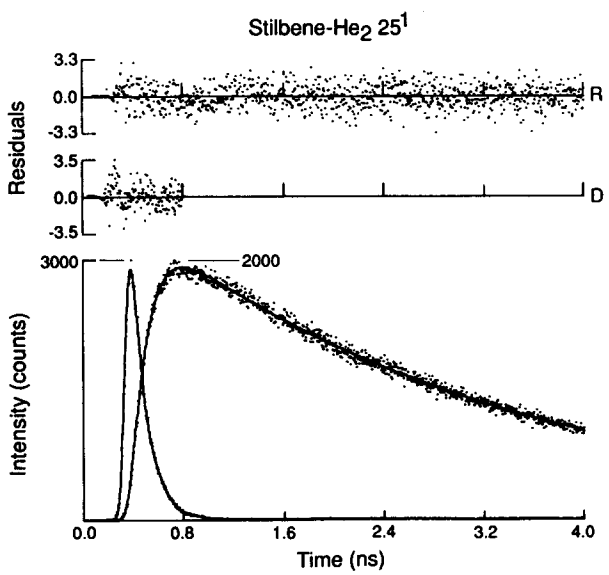

FIG. 13. Temporal data for the decay ($\tau = 90$ ps, $\chi_r^2 = 1.06$) of stilbene–He_2 25^1 fluorescence at 3083.6 Å and a triple exponential fit ($\tau_{IVR} = 94$ ps, amplitude IVR/amplitude fluorescence $= A_{IVR}/A_f = -1.99$, $\tau_{VP} = 42$ ps, $A_{VP}/A_f = 0.97$, $\chi_r^2 = 1.00$) for the fluorescence of the vibrationless stilbene formed.

B. Complexes with neon and argon

Excitation spectra[3] and rotational constants[5] of stilbene–neon and stilbene–argon have been measured. Transitions in the complex to the vibrationless and 198 cm^{-1} states are observed 16 and 63 cm^{-1} to the red of the corresponding stilbene transition for the neon and argon complexes, respectively. An additional band in the spectrum of the argon complex at -40 cm^{-1} with respect to the stilbene transitions is assigned to a transition in the van der Waals modes.[3]

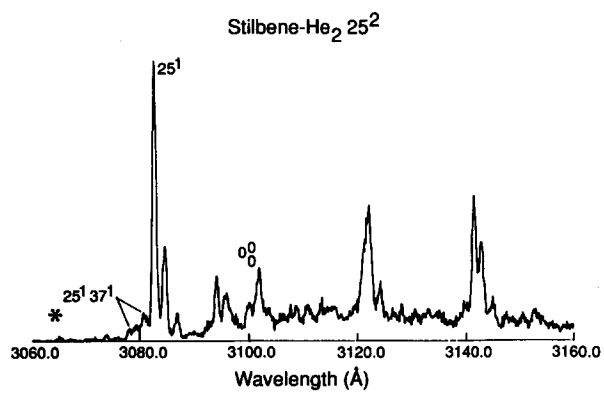

FIG. 15. Dispersed fluorescence spectrum ($R = 0.5$ Å) of stilbene–He_2 25^2. The peak at 3095.5 Å has not been assigned.

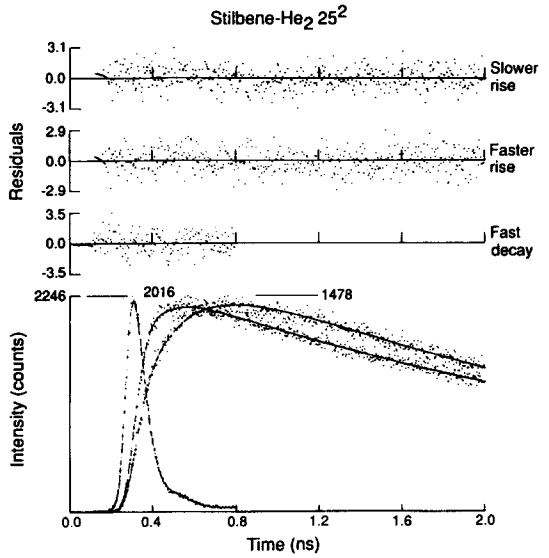

FIG. 16. Temporal data for the decay ($\tau = 36$ ps, $\chi_r^2 = 1.03$) of stilbene–He_2 fluorescence at 3064.9 Å and the rise $\tau = 30$ ps, $\chi_r^2 = 0.99$ in the fluorescence ($\lambda = 3082.5$ Å) of the stilbene 25^1 formed. The data to the right is vibrationless stilbene fluorescence and has a strong ($A_{VP}/A_f = -0.481$) slowly rising ($\tau = 243$ ps) component in the fit ($\chi_r^2 = 1.04$).

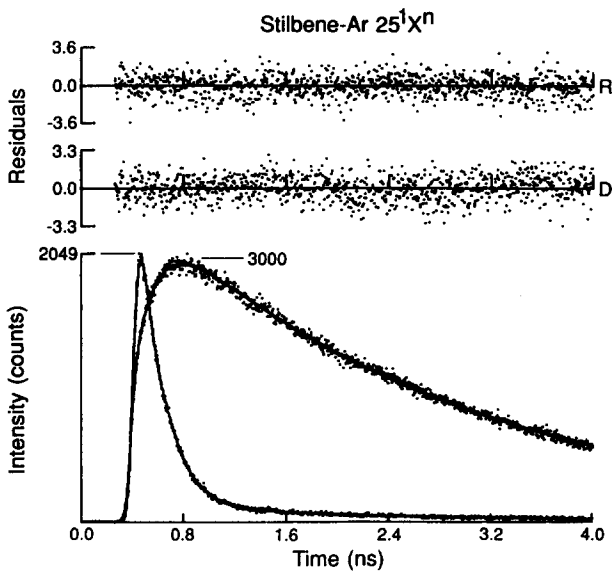

FIG. 18. Temporal data for the decay ($\tau = 158$ ps, $\chi_r^2 = 1.09$) of stilbene–Ar 25^1X^n fluorescence at 3089.7 Å and the rise ($\tau = 157$ ps, $\chi_r^2 = 1.01$) of emission in the broad part ($\lambda = 3127.0$ Å) of the spectrum.

1. Stilbene–Ar

a. 198 and 396 cm^{-1}. The stilbene–argon absorptions at 198 − 63, 198 − 40, and 396 − 63 cm^{-1} with respect to the stilbene origin all give rise to broad, red-shifted, originlike fluorescence (Fig. 17). The resonant fluorescence decays in 250, 159, and 60 ps, respectively, for these bands, and double-exponential decays with the same fast rise times are measured in the broad part of the spectrum (see Fig. 18).

b. 594 cm^{-1}. At this energy the primary product is bare, vibrationless stilbene (Fig. 19). Bands assigned to stilbene 37^1 are also observed above a broad, congested background. At low (8 Å) resolution, the time evolution of the fluorescence from the vibrationless product is well fit by a biexponential with a partial rise time (the ratio of the amplitudes is − 0.7 rather than − 1.0) of 125 ps (Fig. 20). An "internal timing"[11] analysis of the fluorescence spectrum (i.e., relating fluorescence yields to decay lifetimes) indicates that the initial stilbene–Ar vibrational state population decays in < 16 ps.

2. Stilbene–Ne

a. 198 cm^{-1}. The spectrum from the neon complex excited to the level 25^1 shows that the primary product is vibrationless stilbene and that stilbene in the states 36^1 and 37^1 are minor products (Fig. 21). The resonant fluorescence from the complex decays in 233 ps (Fig. 22). The emission from the bare, vibrationless stilbene is well fit as a triexponential with a 233 ps rising component and a 63 ps decaying component in addition to the long, fluorescence decay (Figs. 3 and 22). Amplitudes of the three components are related to the measured lifetimes as will be discussed in Sec. IV B.

As is the case with the minor products of other complexes, it is difficult to spectrally resolve the weak emission of minor products and consequently the measured kinetic pa-

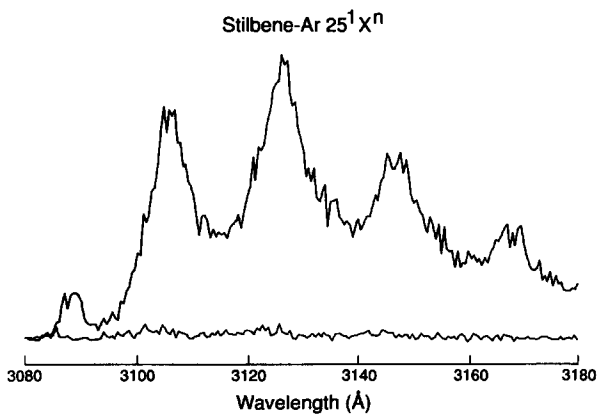

FIG. 17. Dispersed fluorescence ($R = 0.8$ Å) for excitation at the energy of stilbene–Ar 25^1X^n (i.e., 198 − 40 cm^{-1}). The two traces were recorded under identical conditions, except for the small concentration of argon leaked into the molecular beam expansion for the upper measurement.

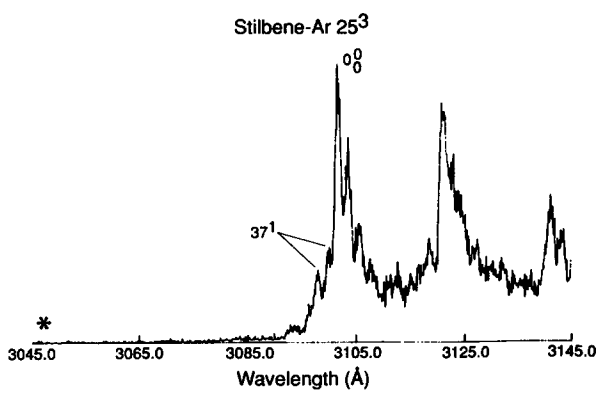

FIG. 19. Dispersed fluorescence spectrum ($R = 0.5$ Å) of stilbene–Ar 25^3. An asterisk marks the excitation wavelength.

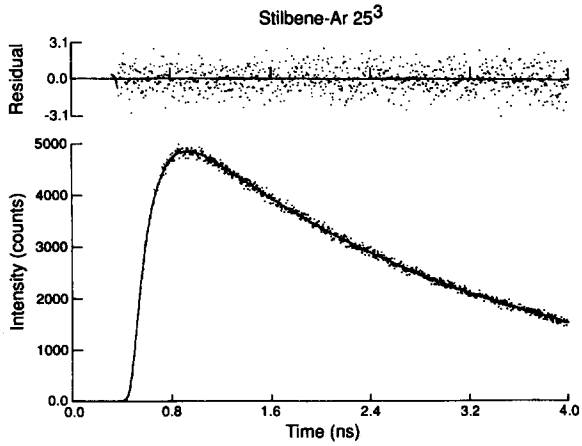

FIG. 20. Temporal data for the product of the reaction: stilbene–Ar 25^3 → stilbene 0^0 + Ar. $R = 8.0$ Å and $\Delta = 88$ ps. The best fit is a biexponential with a 125 ps rise time, $\chi_r^2 = 1.01$.

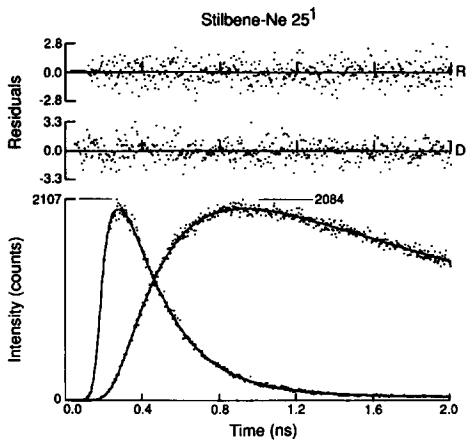

FIG. 22. Temporal data for the decay ($\tau = 233$ ps, $\chi_r^2 = 1.04$) of stilbene–Ne 25^1 fluorescence at 3096.0 Å and a triple exponential fit ($\tau_{IVR} = 233$ ps, $A_{IVR}/A_f = -1.34$, $\tau_{VP} = 65$ ps, $A_{VP}/A_f = 0.36$, $\chi_r^2 = 0.93$) for the fluorescence of the vibrationless stilbene formed.

rameters depend on the spectral resolution. The most highly resolved (spectral resolution, $R = 0.48$ Å) emission from bare stilbene in the 37^1 state could be fit as a double exponential with only a 207 ps rise time. With less spectral resolution ($R = 0.96$ Å), the fluorescence from this state was fit with a partial rise time (i.e., the ratio of amplitudes was -0.5, not -1.0) of 195 ps. These data curves are plotted in Fig. 23 and show the change in the rising component of this emission as the spectral resolution is changed. Since product fluorescence should rise no faster than the decay of the initially excited state (233 ps), it appears this emission is still insufficiently resolved to measure kinetic parameters for this state.

b. 396 cm^{-1}. The fluorescence spectrum of stilbene–Ne excited to the second overtone of ν_{25} is shown in Fig. 24. Bands due to vibrationless stilbene and stilbene 25^1 are marked. Temporal data for some of the more intense bands in the spectrum were recorded with low (4.8–1.6 Å) resolution. All had partial rise times of 116 ps, the same as the decay lifetime of the resonant fluorescence (Fig. 25).

IV. DISCUSSION

A. Preliminary

1. Stilbene spectroscopy and dynamics

The spectroscopy of the vibrational structure of jet-cooled S_1 *trans*-stilbene has been studied before.[2,6,7] The electronic origin is at 3101.4 Å. To the blue there are major absorptions at 83, 95, and 198 cm^{-1} that are important in this work, hot band absorptions (sequence bands from thermally populated low energy levels) at 26 and 39 cm^{-1}, and combinations and overtones of all these bands. The upper levels reached in these transitions are assigned to ν_{25}, an in-plane bend at 198 cm^{-1}; ν_{36}, an out-of-plane bend of the phenyl rings with respect to the ethylene double bond at 35 cm^{-1}; and/or ν_{37}, an antisymmetric torsion of the phenyl rings around the ethylene–phenyl bond at 47.5 cm^{-1}. There are, in addition, two nontotally symmetric modes with vibrational frequencies[12,13] below 200 cm^{-1}, but these play no role in the low energy excitation spectrum in the molecular beam.

The dynamics of jet-cooled S_1 stilbene has also been studied before, by time-resolved spectroscopy. The fluores-

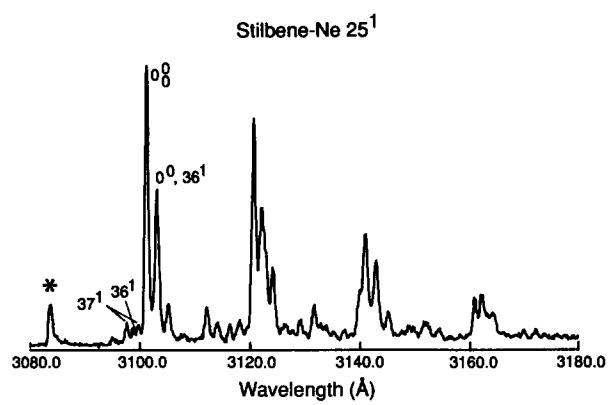

FIG. 21. Dispersed fluorescence spectrum ($R = 0.5$ Å) of stilbene–Ne 25^1. An asterisk marks the excitation wavelength.

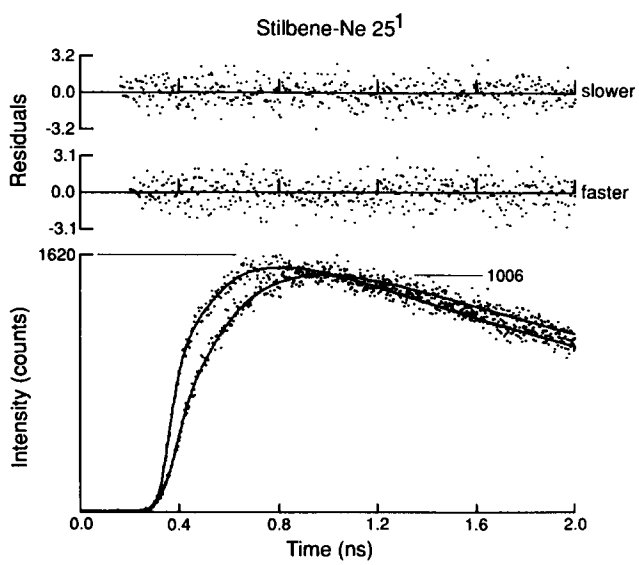

FIG. 23. Dependence on spectral resolution of the temporal data for the weak stilbene 37^1 band at 3097.7 Å in Fig. 21. For the decay with the faster ($\tau = 195$ ps) rise, $R = 1.0$ Å, $\Delta = 88$ ps, $A_{IVR}/A_f = -0.50$, and $\chi_r^2 = 1.08$. For the decay with the slower ($\tau = 207$ ps) rise, $R = 0.5$ Å. $\Delta = 112$ ps, $A_{IVR}/A_f = -0.92$, and $\chi_r^2 = 1.10$.

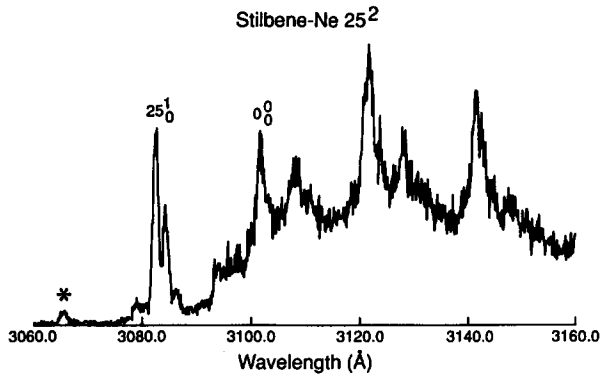

FIG. 24. Dispersed fluorescence spectrum ($R = 0.5$ Å) of stilbene–Ne 25^2. An asterisk marks the excitation wavelength.

cence lifetime is 2.6 ± 0.1 ns for every excitation band below 1200 cm^{-1}, the barrier to isomerization.[10] IVR is not observed[4] until 663 cm^{-1} (quantum beats were observed at the $S_1 + 396$ cm^{-1} excitation in the course of the present studies), and there is no evidence for any other radiationless transition, as evidenced by lifetime and quantum yield measurements.[2,4,14]

2. Geometry of van der Waals complexes

The geometric structure of the complexes of stilbene studied in this work have been studied experimentally by measuring the purely rotational coherence[5] and the high resolution, rotationally resolved excitation spectrum.[15] For each 1:1 complex, the average position of the rare gas atom is between 3.0 and 3.45 Å above the plane of one phenyl ring,

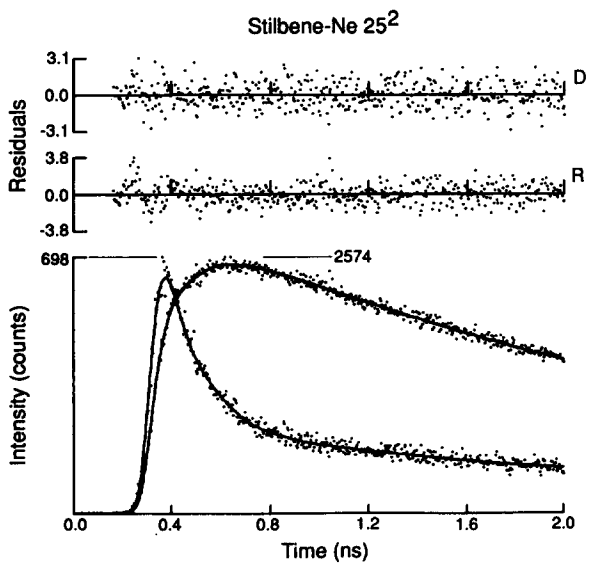

FIG. 25. Temporal data for the decay ($\tau = 111$ ps, $\chi_r^2 = 1.07$) of stilbene–Ne 25^2 fluorescence at 3077.9 Å and for the rise ($\tau = 119$ ps, $\chi_r^2 = 1.03$) of fluorescence from stilbene 25^1. The decay of resonance fluorescence at the excitation wavelength has nearly no long-time component, but could not be fit due to a contribution from scattered laser light.

displaced towards the center of the stilbene molecule between 0.1 and 0.5 Å.

B. IVR and vibrational predissociation: General considerations

1. Parallel and sequential kinetics

In this section, the results of the time-resolved experiments will be analyzed in terms of various kinetic models. Pragmatically this is justified by the fact that all of the data are fit very well by single, double, and triple exponentials and each of these possibilities can be accurately distinguished. Furthermore, as will be shown, these different exponential decays have a simple interpretation, consistent with each other and with the spectral results of these experiments.

In the kinetic model we consider first-order, unimolecular decays of individual vibrational levels due to intramolecular vibrational redistribution to other bound states and decays to continuum states of the dissociated fragments due to vibrational predissociation.

IVR[4] is the process that occurs when *coupled* vibrational states are excited and detected. For example, if a single normal-mode vibrational state with absorption strength were coupled by anharmonicities or Coriolis interactions with a small number of "dark" states and excited coherently so that each of the individual molecular eigenstates were simultaneously excited at $t = 0$, then the population in the absorbing state would flow into and out of the dark modes which are also part of the molecular eigenstates.[16] Kinetic equations cannot explain such behavior. It has been experimentally verified[16] that IVR among a large number of coupled levels may, however, be modeled by kinetic rate equations when the excitation is coherent and the emitting states (but not the eigenstates) are spectrally resolved. In the limit of many coupled levels, the population in the initially excited state decays exponentially with a rate proportional to the width of the distribution of beat frequencies and the population in the "redistributed" states would increase with that same rate. For the analogous process of intersystem crossing, Lahmani *et al.* have shown[17] the correspondence between kinetic analysis and the eigenstate description. Our data will be modeled in this way.

Vibrational predissociation is similar to IVR, except that the "final" states are continuum states of the recoiling fragments. Thus population evolves from an initial zero-order bound state of the molecular complex into a coordinate for which the energy of the system is above the dissociation energy. Fano has shown[18] (for the analogous process of autoionization) that when a discrete zero-order state is coupled to a continuum and prepared coherently, it will dissociate into the continuum with a rate proportional to the strength of the coupling between the zero-order discrete state and the zero-order continuum states. It is therefore reasonable to model VP as a first-order kinetic process.

As the simplest possible mechanism, first consider the kinetics if the initially excited state were to directly decay by several paths. For example, suppose IVR formed a metastable state of the complex which fluoresced and, simultaneously, VP formed the molecular part of the complex in a lower vibrational state which also fluoresced

$$\begin{array}{l} \overset{k_{VP}}{\nearrow} \quad S^* + R \overset{k_f}{\rightarrow} S + R \\ S - R^*_{initial} \overset{k_{IVR}}{\searrow} \\ \qquad\quad S - R^*_{final} \overset{k_f}{\rightarrow} S - R, \end{array}$$

where S is stilbene, R is a rare gas atom, and the asterisk indicates electronic excitation. (For simplicity, the fluorescent decay rates of the initial and intermediate states will be ignored at this point; we also take k_f of the final state $\ll k_{IVR}$ or k_{VP}, which is the case.) Solution of the kinetic equations for this mechanism gives

$$[S - R_i^*(t)] = [S - R_i^*(0)]e^{-(k_{IVR}+k_{VP})t},$$

$$[S^*(t)] = [S - R_i^*(0)]\frac{k_{VP}}{k_{VP}+k_{IVR}-k_f} \times (e^{-k_f t} - e^{-(k_{IVR}+k_{VP})t}),$$

and

$$[S - R_f^*(t)] = [S - R_i^*(0)]\frac{k_{IVR}}{k_{VP}+k_{IVR}-k_f} \times (e^{-k_f t} - e^{-(k_{IVR}+k_{VP})t}).$$

Therefore, the only difference in the two channels reflecting the individual rates appears in the relative proportion of the two products. When these equations are integrated to give the total product state distribution (PSD), the fraction of redistributed complex formed, e.g., is $k_{IVR}/(k_{IVR}+k_{VP})$.

If more decay channels are open to the initial state, the form of the kinetic equations is the same: the temporal evolution of the initial state is a single exponential with the total decay rate and each product state population evolves as a biexponential rising with the same rate. The amount of each product formed is determined by the ratio of the rate for that channel to the total rate.

In contrast, the temporal results differ in functional form if the decay processes occur sequentially. For example, if IVR preceded VP and the bare molecular product fluoresced (again ignoring the fluorescence rates of the complex levels for simplicity)

$$S - R^*_{initial} \overset{k_{IVP}}{\rightarrow} S - R^*_{final} \overset{k_{VP}}{\rightarrow} S^* + R \overset{k_f}{\rightarrow} S + R,$$

a general result is that each state involved in the dissociation process would have a temporal behavior described by a sum of exponentials, one for each rate process which preceded it and another for its decay rate.[19] In the given example,

$$[S - R_i^*(t)] = [S - R_i^*(0)]e^{k_{IVR}t},$$

$$[S - R_f^*(t)] = \frac{k_{IVR}}{k_{VP}-k_{IVR}}[S - R_i^*(0)](e^{-k_{IVR}t} - e^{-k_{VP}t}),$$

$$[S^*] = \frac{k_{IVR}k_{VP}}{(k_f-k_{VP})(k_f-k_{IVR})}[S - R_i^*(0)]\left\{e^{-k_f t} + \frac{k_f-k_{VP}}{k_{VP}-k_{IVR}}e^{-k_{IVR}t} + \frac{k_f-k_{IVR}}{k_{IVR}-k_{VP}}e^{-k_{VP}t}\right\}.$$

The emission of the bare molecule (which has a relatively long lifetime in these experiments) *would be a triple exponential* with a rise time equal to the slower of the IVR and VP rates. The faster of these and the fluorescence rate appear as the rates of two decaying components. The amplitudes of the components of the triexponential are not equal in magnitude as they are for the biexponentials that are observed if the kinetics are parallel, but are functions of k_{IVR}, k_{VP}, and k_f.

For sequential IVR and VP then, the rise time of product fluorescence may be equal to *or slower* than the decay time of the initial state. In either case, the temporal behavior of the final product is no longer biexponential (although it appears to be if the temporal resolution is too slow to resolve the fast, additional decay).

A priori, there is no reason to assume the dissociation mechanism will be either only parallel or only sequential, rather than involving some of each simple mechanism. For example, after redistribution to a level including excited van der Waals modes, predissociation could occur to different final states with different rates

$$\begin{array}{l} \overset{k_{IVP}}{\rightarrow} \quad \overset{k_{VP}}{\nearrow} \quad S_1^* + R \overset{}{\rightarrow} S_1 + R \\ S - R^*_{initial} \rightarrow S - R^*_{final} \overset{k_{VP2}}{\searrow} \quad S_2^* + R \overset{k_f}{\rightarrow} S_2 + R. \end{array}$$

In this case, the kinetic behavior of the states involved would be similar to the behavior for predissociation occurring to only a single state. Specifically, triexponentials would be observed for the final states. As discussed for parallel kinetics, however, k_{VP1} and k_{VP2} would always be observed in the rates as the sum. Again, the only effect of those individual rates would be in the product state distributions. The fraction of product from the first channel, e.g., is $k_{VP1}/(k_{VP1}+k_{VP2})$.

The most general mechanism involving these ideas would be redistribution of the initial state to a number of states, each of which could independently predissociate:

$$
\begin{array}{lll}
 & & \overset{k_{VP1}}{\nearrow} S^*_{1,1} + R \overset{k_f}{\rightarrow} S_{1,1} + R \\
 & S - R^*_{\text{final}(1)} & \overset{k_{VP2}}{\searrow} \\
\overset{k_{IVR1}}{\nearrow} & & \vdots \quad S^*_{1,2} + R \overset{k_f}{\rightarrow} S_{1,2} + R \\
S - R^*_{\text{initial}} & \overset{k_{IVR2}}{\searrow} & \\
\vdots & & \overset{k_{VP3}}{\nearrow} S^*_{2,3} + R \overset{k_f}{\rightarrow} S_{2,3} + R \\
 & S - R^*_{\text{final}(2)} & \overset{k_{VP4}}{\searrow} \\
 & & \vdots \quad S^*_{2,4} + R \overset{k_f}{\rightarrow} S_{2,4} + R
\end{array}
$$

As with the simple parallel decay mechanism, the decay rate of the initial state is equal to the sum of IVR rates into the different channels and each channel will have a PSD proportional to the ratio of the rate into that channel to the total rate. As with the simple sequential mechanism, the temporal behavior of each dissociated product will be a triexponential which will rise with the slower of the VP rate out of the intermediate state which preceded it and the total IVR rate out of the initially excited state. What is new in this mechanism is that *different product states of the bare molecule may have different rise times*, reflecting different total rates of predissociation, if the redistribution rate out of the initially excited state is comparatively fast.

Integrating these equations to find the product state distribution and taking k_f to be small compared to k_{IVR} and k_{VP}, one finds that the contribution of the initial, the redistributed, and the dissociated state to the fluorescence spectrum is proportional to its lifetime, and when several channels are open, to $\approx k_i/\Sigma_i k_i$.

Our conclusions on the role of IVR in the dissociation process are based on this analysis. They are:

(1) If the product fluorescence is a biexponential with a rise time equal to the decay rate of the initially excited state, then only a single process may be inferred, though it may consist of any number of parallel channels. The reaction mechanism may still have more than one step, but only the first is resolvable.

(2) If more than one rate is observed, the reaction mechanism must have more than one step, e.g., IVR precedes VP. This could occur by observing (a) a single triexponential for a single stilbene product, (b) two stilbene products with different rise times reflecting different VP rates from different intermediate states and unresolvably fast third components, or (c) a product stilbene decay that has a rise time (VP) slower than the decay of the initially excited state (IVR).

In this paper, we assume that all the initially excited levels and redistributed levels of the complex have the same fluorescence lifetime as the vibrationless level (2.7 ns) and account in our analysis for the effect of this additional parallel channel on the temporal evolution observed. Since the fluorescence rate is small in these experiments compared with the rates we measure for IVR and VP, this effect is minimal. The observed rates generally differ from the kinetic rates by a few percent.

We have also evaluated the effect of reversibility in the redistribution step. Generally, the effect of this reversibility is to make the time evolution of the initial state a biexponential with two decaying components and to make the time evolution of the product stilbene a sum of four exponential terms. Our data has been accounted for more simply, suggesting that the IVR we observe is irreversible.

2. IVR and the van der Waals vibrational state density

Two parameters are necessary to quantify IVR: coupling strengths and vibrational state densities. Felker *et al.*[4,16] have directly measured coupling strengths of ~ 1.0 GHz in bare stilbene by measuring beat frequencies in the fluorescence decays of single vibrational levels. The calculated vibrational state density at energies where dissipative IVR is observed is > 150 per cm^{-1} per symmetry class (accounting for the symmetry restrictions in the coupling). To discuss the role of IVR in these experiments, therefore, we need to consider the effects of the van der Waals modes on the vibrational state density (ρ) of these complexes. Our method is similar to Ewing's.[20]

Models of the van der Waals potential between rare gas atoms and aromatic molecules have exclusively been based on two-body interaction potentials between the rare gas atom and each atom of the aromatic molecule.[21,22] Baskin and Zewail[5] have used structural data on these complexes to evaluate approximately the validity of these calculated potentials in determining rotational constants. Qualitative agreement is found between the experimentally determined structure and that calculated from a sum of two-body potentials in which the aromatic and aliphatic carbons are characterized by different parameters. We used this potential[5] to calculate the density of van der Waals vibrational states. These potentials have double minima, one above each phenyl ring, with a substantial barrier ($\sim 1/4D_e$) between them.

The three coordinates involving motion of the rare gas atom were assumed to be the stretching motion of the atom towards and away from the phenyl ring, a bending motion parallel to the line on which the double minima occur and a bending motion perpendicular to that line. As an example, plots of the vibrational potential energy along these three coordinates are shown in Fig. 26 for stilbene–Ar, along with the fits of these curves to a Morse potential and two $1/\cosh^2 x$ potentials, respectively, each of which is determined by a well depth and a range parameter.[23] Only a single well of the double minimum potential was fit for the purpose of calculating the vibrational state density. [No attempt was made to redo the calculation with the double well and higher short-axis bending (and stretching) frequencies because of uncertainties in other parameters such as the anharmonicity and the atom–atom potential.] Vibrational frequencies and anharmonicities for these van der Waals modes were then calculated from the range parameter of the fit and the experimental dissociation energy. The fact that stilbene in the vibrational state 37^1 is produced in the dissociation of stilbene–He excited to 95 cm^{-1}, stilbene–Ne excited to 198 cm^{-1}, and stilbene–Ar excited to 594 cm^{-1} gives experimental upper limits for the dissociation energies of those

complexes of 48, 150, and 546 cm^{-1} respectively. The only experimental lower limit measured is for the argon complex 396 cm^{-1}. The parameters, including cross anharmonicities discussed below, used in the calculations of ρ for the three 1:1 complexes are listed in Table I. Note the similarity in the three sets of calculated van der Waals frequencies.

Treating each coordinate as separable would lead to dissociation only when the energy in any single coordinate exceeded D_0. By adding appropriate cross anharmonicities [e.g., $g_{xy} = 2\sqrt{(g_{xx}g_{yy})}$, where g_{xx}, e.g., is the anharmonic constant for the x coordinate], however, the expression for the van der Waals vibrational energy can be made to reflect dissociation whenever the total energy exceeds D_0. To calculate the energies of the different van der Waals modes, therefore, we used the expression

$$E_{vdW} = \omega_x(n_x + \tfrac{1}{2}) + \omega_y(n_y + \tfrac{1}{2}) + \omega_z(n_z + \tfrac{1}{2}) - g_{xx}(n_x + \tfrac{1}{2})^2 - g_{yy}(n_y + \tfrac{1}{2})^2 - g_{zz}(n_z + \tfrac{1}{2})^2 - g_{xy}(n_x + \tfrac{1}{2})(n_y + \tfrac{1}{2}) - g_{xz}(n_x + \tfrac{1}{2})(n_z + \tfrac{1}{2}) - g_{yz}(n_y + \tfrac{1}{2})(n_z + \tfrac{1}{2}),$$

where the ω's are the vibrational frequencies, the g's are the anharmonic constants, and the n's are vibrational quantum numbers. This expression was used to directly count the number and density of bound levels in the van der Waals well. Because the point group symmetry of the assumed structures of the complexes is C_1, there are no symmetry restrictions for the coupling and all vibrational levels are included in these counts.

A vibrational energy level diagram of S_1 stilbene below 200 cm^{-1} has been constructed using the experimental frequencies of ν_{25}, ν_{36}, and ν_{37}, and the calculated frequencies[12] of 88 and 131 cm^{-1} for ν_{48} and ν_{72}, respectively. This is shown in Fig. 27. The energies of the chemical vibrations of S_1 stilbene–He, assuming $D_0 = 48$ cm^{-1}, and the total density of bound vibrational states, including van der Waals modes, as a function of excess vibrational energy for that complex are also shown. The total vibrational state densities of stilbene–neon and stilbene–argon were calculated in the same way and plots of those functions are shown in Fig. 28. [Use of experimental values reported recently[13] for ν_{48} and ν_{72} (100 and 112 cm^{-1}) instead of the calculated values would have little effect on these densities.]

C. Interpretation of results for stilbene–Ne 25[1]

1. Separation of IVR and VP

The temporal data for stilbene–neon excited to 198 cm^{-1} offers the clearest and the most convincing proof we have that IVR is preceding VP despite the fact that there is no hint of IVR in the time-integrated (i.e., spectral) results. A triexponential with clearly resolved lifetimes is measured in the fluorescence from the product stilbene, and a matching decay of fluorescence from the initially excited state is also observed. From this data we can identify 1/(255 ps) (correcting for k_f) as the total rate of dissipative IVR from the initially excited chemical vibrational level of the complex and 1/(65 ps) (correcting for k_f) as the total VP rate of the intermediate state that precedes the formation of vibrationless stilbene. In this section, we will discuss these two rates in some detail, comparing them with theoretical expectations.

In bare stilbene, dissipative IVR is not observed until 1237 cm^{-1} and no IVR is observed at only 198 cm^{-1} of excess energy. It is perhaps surprising that the weak binding

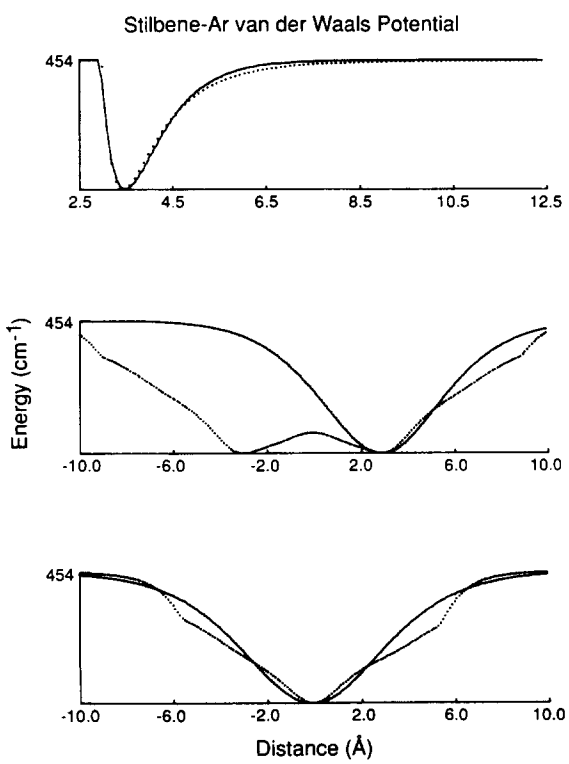

FIG. 26. Sections of the van der Waals potential energy surface between stilbene and argon along the van der Waals normal coordinates and the fits of these sections to a Morse potential and two $1/\cosh^2 x$ potentials.

TABLE I. Calculated van der Waals frequencies and anharmonicities (in wave numbers).

Stilbene–Ar				
	$\omega_x = 8.06$	$g_{xx} = 0.032$	$g_{xy} = 0.073$	
	$\omega_y = 9.21$	$g_{yy} = 0.042$	$g_{xz} = 0.334$	$D_0 = 478$[a]
	$\omega_z = 42.00$	$g_{zz} = 0.87$	$g_{yz} = 0.381$	
Stilbene–Ne				
	$\omega_x = 6.34$	$g_{xx} = 0.058$	$g_{xy} = 0.133$	
	$\omega_y = 7.26$	$g_{yy} = 0.076$	$g_{xz} = 0.604$	$D_0 = 150$[b]
	$\omega_z = 32.96$	$g_{zz} = 1.57$	$g_{yz} = 0.691$	
Stilbene–He				
	$\omega_x = 9.14$	$g_{xx} = 0.267$	$g_{xy} = 0.611$	
	$\omega_y = 10.46$	$g_{yy} = 0.349$	$g_{xz} = 2.78$	$D_0 = 48$[b]
	$\omega_z = 47.56$	$g_{zz} = 7.22$	$g_{yz} = 3.17$	

[a] Approximately the average of the experimental upper and lower limits.
[b] Experimental upper limit.

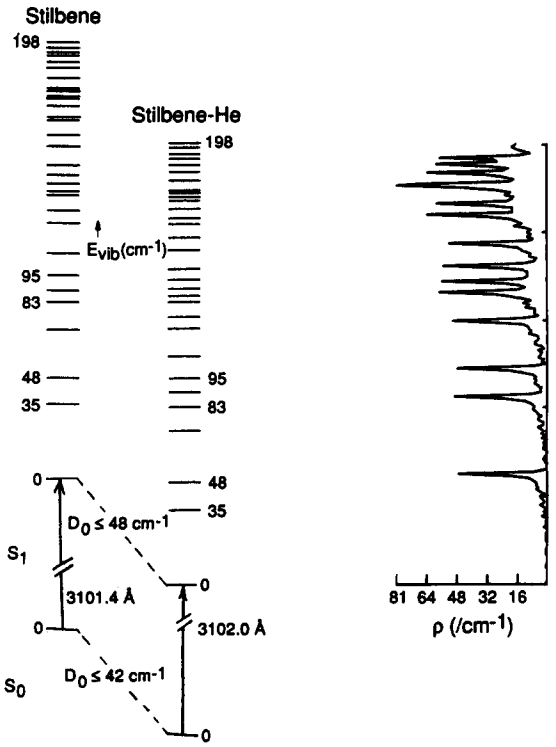

FIG. 27. Vibrational energy level diagram for stilbene and stilbene–He. The "stilbene-like" or chemical vibrational levels of the complex are shown for an assumed D_0 of 48 cm^{-1}. To the right is a plot of the total density of vibrational levels in the complex, including van der Waals levels. The sharp peaks in the state density occur as the energy in the van der Waals modes in combination with each stilbene vibration approaches D_0.

($D_0 \leqslant 198$–48 cm^{-1}) of a rare gas atom can affect the relaxation dynamics of this in-plane vibrational mode so drastically.

The vibrational state density of stilbene–neon at 198 cm^{-1} is seen in Fig. 28 to be 330 per cm^{-1}. This value

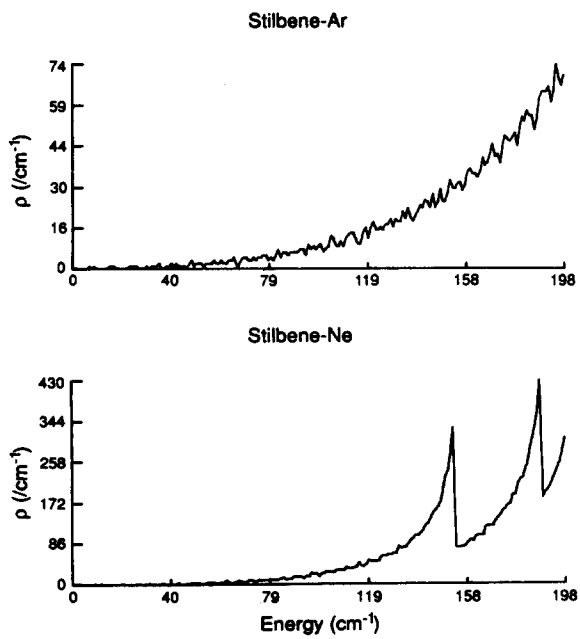

FIG. 28. The total density of vibrational states in stilbene–Ne and stilbene–Ar including the full anharmonicity of the van der Waals modes as in Fig. 27.

can be compared to the state density at which dissipative IVR is first observed in bare stilbene (150 per cm^{-1}). According to theory,[16,17] the intramolecular dephasing of a bound state (as is the case for IVR) approaches a single exponential form more closely as the number of coupled levels increases and the decay rate of the dephasing is given by a golden-rule type expression. Thus, comparing state densities for the bare molecule and the complex and assuming for the moment that the coupling strengths are similar ($\sim$1.0 GHz), we would expect the IVR dephasing in the complex to be more nearly dissipative (i.e., no or fewer recurrences) and the decay rate to be $\sim 2\pi \overline{V}^2 \rho = 1/(14\ \text{ps})$. Thus, the rate calculated for this approximate value of $\overline{V}$ and the full vibrational state density is more than an order of magnitude faster than the observed IVR rate.

2. Vibrational predissociation—Comparison with theory

As discussed above, we can identify 1/(65 ps) as the total VP rate from some redistributed level at 198 cm^{-1} in stilbene–Ne. We can compare this experimental VP rate with rates calculated according to statistical rate theories[24] and according to the momentum-gap law.[20,25]

Classical RRK theory gives

$$k = A\left(\frac{E - D_0}{E}\right)^{S-1},$$

where E is the energy of the undissociated molecule, D_0 the dissociation energy, S the number of oscillators in the molecule, and A is the frequency of the van der Waals stretch (i.e., the reaction coordinate). Taking the IVR to be complete so that all eight normal modes (three van der Waals modes and five stilbene modes) with fundamental frequencies up to 198 cm^{-1} take part in the dissociation, and taking 150 cm^{-1} as D_0, we calculate a predissociation lifetime at 198 cm^{-1} of 20 ns for stilbene–Ne, orders of magnitude different from the experimental value. Similarly, the classical RRK approach gives a state density for stilbene–Ne at 198 cm^{-1} of

$$\frac{E^{S-1}}{(S-1)!\,\Pi_{i=1}^{s}\, h\nu_i} = 0.40\ \text{cm}^{-1},$$

where ν_i is the frequency of the i^{th} oscillator. Comparing this value of the vibrational state density with the value calculated by directly counting anharmonic levels, the discrepancy is clear.

RRKM rate constants are given by the expression

$$k(E) = N^{\dagger}(E)/h\rho(E),$$

where k, E, and ρ are as before and $N^{\dagger}$ is the number of levels of the transition state. The van der Waals stretching mode of the stilbene complex was assumed to be the reaction coordinate. For simplicity, all other modes were assumed the same in the transition state as in the excited complex (tight transition state). Harmonic frequencies of 40.0, 9.0, and 8.0 were used in the calculation for the van der Waals modes (compare with Table I). The RRKM rates were calculated by directly counting harmonic vibrational levels as discussed by Khundkar *et al.*[24] who have previously applied this theory to dissociation of van der Waals complexes. Such an approach has also been applied to other systems.[26] Here, some

rates were calculated with anharmonicities included for the van der Waals modes to evaluate the accuracy of the calculation. Calculated and observed VP rates for the major products of several different complex dissociations are given in Table II.

The VP lifetime for stilbene–neon at 198 cm^{-1} calculated from RRKM theory using a harmonic count of vibrational levels is 75 ps. The lifetime increases to 97 ps when anharmonic levels are counted and D_e is taken to be 250 cm^{-1}. D_e determines the anharmonicities in the anharmonic model and differs from D_0 by about 25 cm^{-1} in this case. The value used is somewhat higher than the experimental upper limit of ~ 175 cm^{-1} so that a vibrational state density of bound levels in the complex at 198 cm^{-1} can be calculated. Including cross anharmonicities also, but counting only the bound states below the dissociation limit, the calculated lifetime is 239 ps.

Our experimental VP rate of 1/(65 ps) can also be compared to theoretical expectations according to the momentum-gap law. As developed by Ewing,[20,25] this law can be derived by separating the matrix element in Fermi's Golden Rule into a factor involving the van der Waals states and a factor involving the chemical vibrations. The factor involving the chemical vibrations in the matrix element is similar to an infrared transition matrix element and is fully allowed for $\Delta v = 1$, and less allowed for $\Delta v = 2$, 3, etc. For a slowly changing van der Waals potential, the van der Waals factor in the matrix element is a Franck–Condon overlap integral between the initial van der Waals state and the outgoing plane wave function for the predissociated atom. Without van der Waals mode excitation, low translational energy products are favored, i.e., there is a low "energy-gap" propensity. For an initial state with excited van der Waals modes (particularly the stretch), however, Ewing[20] has shown that the energy gap may be compensated for, in a sense, since the greater number of nodes in the van der Waals vibrational wave function can maximize the overlap integral with a relatively high energy plane wave eigenfunction for the translational state of the final fragment. The above factors, momentum gap and vibrational changes, determine the momentum-gap rate, but the relative importance of each cannot be judged without explicitly calculating matrix elements and overlap integrals for the potential energy surface of the complex.

Ewing has simplified these results to give[11b,20]

$$k_{\mathrm{VP}} = 10^{13} e^{[-\pi(\Delta n_t + \Delta n_v)]},$$

$$\Delta n_t = \frac{\sqrt{2\mu \Delta E}}{2a\hbar} - v_z,$$

where Δn_v is the change in chemical vibrational quantum numbers, Δn_t is the change in the "translational quantum number," μ is the reduced mass of the fragments, ΔE is the final relative translational energy of the fragments, a is the Morse potential range parameter, $\hbar$ is Planck's constant, and v_z is the vibrational quantum number for the van der Waals stretching mode. Since 37^1 stilbene is a product of the dissociation of stilbene–neon 25^1, ΔE can be no less than 48 cm^{-1} for the formation of vibrationless stilbene if all the available energy goes into translation. (Although the partition of kinetic energy between translation and rotation is not known, a simple calculation for impulsive dissociation predicts that more than 90% of the available energy appears as translational kinetic energy.) Taking 50 cm^{-1} as the value of ΔE, the range parameter (1.3 $Å^{-1}$) calculated from the van der Waals potential and taking $\Delta n_v = 1$ since low overall Δn channels are favored in the experimental product state distributions, this equation gives VP rates of between 21 ns and 3.1 ps depending on whether the van der Waals stretching mode is in the $v_z = 0$, 1, 2, or 3 state. The rate for $v_z = 2$ is listed in Table II. Clearly, the rate predicted by the momentum-gap law cannot be tested against the experimental

TABLE II. Calculated and observed vibrational predissociation lifetimes.

	τ_{VP} (observed) (ps)	τ_{VP} (RRKM) (ps)	τ_{VP} (m-g)[a] (ps)
S–Ne 198 cm^{-1}	65	75 ($D_0 = 150$ cm^{-1})[b]	40
		12 ($D_0 = 100$ cm^{-1})	
S–Ne 396 cm^{-1}	<20?[c]	8.4 ($D_0 = 150$ cm^{-1})[b]	40[d]
S–Ar 594 cm^{-1}	125	146 ($D_0 = 396$ cm^{-1})[e]	1200
		1400 ($D_0 = 500$ cm^{-1})	
S–He_2 198 cm^{-1}	43	42 ($D_0 = 96$ cm^{-1})	2
S–He_2 396 cm^{-1}	<20?[c]	7 ($D_0 = 96$ cm^{-1})	
S–He 83 cm^{-1}	f	12 ($D_0 = 48$ cm^{-1})	0.3
S–He 95 cm^{-1}	f	10	
S–He 198 cm^{-1}	f	3	
S–He 396 cm^{-1}	f	2	

[a] Momentum-gap lifetime, taking $\Delta E = 50$ cm^{-1}, $v_z = 2$, $\Delta n_v = 1$.

[b] Experimental upper limit for D_0.

[c] No lifetime attributable to VP was resolved.

[d] The momentum-gap lifetime does not depend explicitly on initial energy.

[e] Experimental lower limit for D_0.

[f] For this complex, IVR and VP lifetimes could not be distinguished.

value without knowledge of the intermediate state. General statements will be made, however, in the next section when different rates are compared.

D. Other results

The results for the other excitations and other clusters support these conclusions about IVR and VP in the dissociation process directly or indirectly. For example, the data for the three excitations of ν_{25} (25_0^1, 25_0^2, and 25_0^3) in stilbene–Ar strongly suggest the dissociation is a two-step process, that IVR precedes VP. At 25^1 and 25^2, rates of irreversible IVR of 1/(250 ps) and 1/(60 ps), respectively, are measured from the broad fluorescence (itself the *spectral* signature of dissipative IVR). At 25^3, where the IVR rate is apparently too fast to resolve, narrow bands assigned to bare, vibrationless stilbene have a 125 ps rise which we attribute to the total VP lifetime from some redistributed level. Both the RRKM and the momentum-gap theories predict a longer decay lifetime for this reaction compared to the decay lifetimes calculated for stilbene–Ne 25^1. These lifetimes are listed in Table II.

For the 25^2 excitation of stilbene–Ne, only one rate, the decay rate of the initially excited state, was actually resolved. A comparison of this rate with other IVR rates for the neon and argon complexes studied and the fact that the calculated RRKM rate (Table II) is significantly faster than the RRKM rate for 25^1 excitation suggests that the dynamics of this level is only faster than the dynamics for the 25^1 level, not different. Note also that the congestion in the red part of the dispersed fluorescence spectrum is likely to conceal any different behavior in the temporal profile of fluorescence from vibrationless stilbene.

For the 25^1 excitation of stilbene–He_2, not only was a triexponential decay of the fluorescence from vibrationless stilbene measured, but a different rise time was measured for the product 37^1 stilbene. Each of these observations is evidence for a multistep process. Based on the redistribution rates seen in other complexes, we interpret the 90 ps decay of the initial state as IVR, but it is also possible that the observed behavior results from a sequential dissociation of this 1:2 complex described by

$$S - He_2^* \xrightarrow{k_{VP1}} S - He^* + He \xrightarrow{k_{VP2}} S^* + 2He \xrightarrow{k_f} S + 2He.$$

The detailed dynamics from the different excitations of the stilbene–He complexes are the least clearly understood of the systems we have studied. Without knowing the decay rate of the initially excited state, it is not clear whether or not IVR is occurring from these levels. One possibility is that the states which predissociate to form 37^1 and 0^0 stilbene are separated by ~ 1 cm^{-1}, but both derive their absorption strength from the zero-order state, stilbene–He 37^2. In this case, IVR would necessarily precede VP with our laser. On the other hand, recent work by Zwier[3(c),27] on stilbene–H_2 and *p*-methylstilbene–H_2 suggests that the broadening may be from unresolved vibrational structure in the van der Waals modes. In this case, the initially excited states could independently predissociate, without IVR, also consistent with our results.

Excitation of 25^1 and 25^2 in the stilbene–He complex yields an unassignable spectrum with no third component in the temporal profile of the fluorescence. However, very fast VP rates are calculated (see Table II) for this complex according to both RRKM theory (because of the small value of D_0) and according to the momentum-gap law (because of the small reduced mass of the complex). It is doubtful that the decay rates measured are due to direct VP from the initially excited chemical vibrational level when those channels are not observed for the other complexes studied.

1. Product state distributions

When more than one product is formed in the dissociation, the experimental PSDs give information on rate processes that occur in parallel. According to the kinetic model, the time-resolved data can determine whether the parallel process occurs in the IVR step or the VP step. If different VP lifetimes are measured, as is the case for stilbene–He_2 25^1 and 25^2, then different intermediate states are formed in the IVR step, and predissociate independently. Assuming no branching in the VP step from the intermediate states, the PSD can be used to calculate individual IVR rates. Conversely, if identical triexponentials are measured for different final states, it is likely that the different products are formed in the VP step and the PSD would be determined by the individual VP rates (since, *a priori*, one would not assume identical VP rates from different intermediate states).

For stilbene–Ne and stilbene–Ar, the signal was insufficient to accurately measure temporal data for minor products at the high spectral resolution necessary to isolate individual bands. Assuming, therefore, similar dissociation paths, i.e., IVR to different states which VP independently, the IVR rates for all of these excitations were calculated by taking the relative emission intensities to be proportional to the relative rates, while the total rate (including a fluorescence rate assumed to be the same as that of the bare molecule) was measured. These individual IVR rates are shown in Table III. This table does not include stilbene–He data since the PSDs observed from that complex either depended on the precise excitation frequency within the inhomogeneous excitation band or could not be assigned.

2. Comparison of linewidths and measured lifetimes

The stilbene–He complex is the only large polyatomic-rare gas van der Waals complex that has been studied by measuring both excitation linewidths[3] and by directly time resolving the population of reactants and products (Ref. 1 and here). The bands in the excitation spectrum of the stilbene–He complex at 83 and 95 cm^{-1} are unusually broad compared to other complex bands, having a full width at half maximum of ~ 3 cm^{-1}. If homogeneous, this width corresponds to a lifetime of ~ 2 ps. In these time-resolved experiments, however, we measured product rise times of 36 and 42 ps, respectively, for those two transitions. It is apparent that the broad excitation linewidths do not accurately reflect the dissociation rates, as emphasized by us[1,16] and by Gentry.[28]

Originally, both our work[1] and the work of Zwier and

TABLE III. Observed product state distributions and lifetimes

Energy	Product state	τ_{IVR} (ps)[a]	τ_{VP} (ps)	PSD
Stilbene–He_2				
198 cm^{-1}	0^0	129	43	72%
	36^1	621	?	15%
	37^1	716	~150	13%
396 cm^{-1}	0^0	236	~270	~15%
	25^1	45	<20	77%
	25^137^1	443	?	8%
Stilbene–Ne				
198 cm^{-1}	0^0	445	65	56%
	36^1	850	?	30%
	37^1	1821	?	14%
396 cm^{-1}	0^0	379	?	32%
	25^1	209	<20	58%
	25^137^1	1212	?	10%
Stilbene–Ar				
198 cm^{-1}	?	276	...	...
198 + 23 cm^{-1}[b]	?	169	...	...
396 cm^{-1}	?	61	...	...
594 cm^{-1}	0^0	<20	125	~80%
	37^1	<20	?	~20%

[a]These lifetimes are calculated from measured IVR rates (corrected for k_f) and the product state distributions (PSDs).
[b]The band in the excitation spectrum at -40 cm^{-1} with respect to the 198 cm^{-1} band in bare stilbene.

co-workers[3(b)] suggested that the broad lines in the excitation spectrum could be due to fast IVR out of the initially excited state, preceding dissociation. However, the dependence of the PSD on the precise excitation wavelength reported here for the 83 and 95 cm^{-1} bands and reported by Zwier[3(c)] for the 95 cm^{-1} band show that the absorption bands are inhomogeneously broadened. The identity of the states within the inhomogeneous width and the time scale for energy flow between them is still not resolved. As discussed elsewhere,[29] the contribution of homogeneous and inhomogeneous broadenings must be separated before deducing the dynamics.

3. Mode specificity

In these experiments, we have directly observed a vibrational mode dependence in the unimolecular dissociation of a large polyatomic system stilbene–He. The dissociation from modes involving ν_{36} and ν_{37} is considerably faster than from modes involving only the higher energy vibration ν_{25}.

A number of possible explanations for this behavior can be considered:

(1) The IVR rate is mode dependent because changes in the displacements of the normal coordinates of ν_{36} and ν_{37} cause large changes in the van der Waals potential energy (these bending coordinates in stilbene have large components along the van der Waals stretch). Weber and Rice[30] suggested that this is the reason for the unusual activity of mode 16a in the dynamics of S_1 tetrazine–Ar. As in that case, the *vibrational* shifts of complex bands including ν_{36} and ν_{37} in the excitation spectrum[3] are different from the vibrational shifts of other bands, though the difference is small.

(2) The VP rate is mode dependent because of a low energy gap propensity. The rate from mode 25 could be slow compared to the rate from the lower energy modes because the stilbene molecules excited to the unassigned product mode must be translationally hot to compensate for a large gap in energy (or relative momentum) between the initial and final states of the reaction.

(3) Both ν_{36} and ν_{37} and the van der Waals vibrations have large amplitudes compared to most chemical vibrations. This will have the effect of increasing the coupling strength and making higher-order anharmonicities more important for both IVR and VP.

(4) The similarity of the frequencies of ν_{36} and ν_{37} to the van der Waals stretching mode may increase the effectiveness of the coupling of these modes for either the IVR or VP.

The nature of these levels in the neon and argon complexes is less well understood. Zwier reported[3(b)] the absence of bands involving ν_{36} and ν_{37} in the excitation spectra of these complexes, suggesting they were so broadened by IVR that they could not be detected. This was consistent with our observation of weak, broad fluorescence, independent of the precise (i.e., ± 10 cm^{-1}) excitation wavelength in the region of the excitation spectrum where these bands would be expected. Zwier's latest work,[3(c)] however, tentatively identifies narrow bands with unusual shifts with these transitions.

Mode specific rates are also observed in two cases for the VP rates of different products from different, isoenergetic, redistributed levels of the complex. Stilbene–He_2 excited to 25^2 yields 25^1 and 0^0 stilbene with different VP rates (see Table III). According to the kinetic scheme in Sec. IV B, these different rates reflect different VP rates from different intermediate states. Since the identity of these intermediate states is unknown, however, these rates cannot be compared even qualitatively with predictions according to the momentum-gap law, as has been discussed for stilbene–Ne 25^1. In contrast to the two VP rates measured for stilbene–He_2 25^2, it is interesting that the higher energy product of the dissociation of stilbene–He_2 25^1 (37^1, τ_{VP} ~140 ps) is formed more slowly than the lower energy product (0^0, τ_{VP} ~43 ps). In both cases, the product formed with the faster rate differs from the initial state by the smaller number of vibrational quanta, not by the smaller energy gap.

V. CONCLUSIONS

This paper includes experimental results of the direct, time-resolved measurements of the population of both the products and initial states in the unimolecular dissociation of the van der Waals complexes of stilbene with helium, neon, and argon excited to combinations and overtones of ν_{25}, ν_{36}, and ν_{37}.

We have studied the time-resolved dynamics of 14 excited vibrational levels of these complexes. The time-resolved data for the complexes stilbene–Ne, stilbene–Ar, and stilbene–He_2 clearly show that vibrational redistribution precedes vibrational predissociation, even though there is no evidence of redistribution in the spectral data. We have measured fluorescence spectra and lifetimes for six levels of stil-

bene–He, but have not been able to resolve any experimental evidence for a multistep dissociation for that complex. The measured lifetimes do show, however, that the dissociation for that complex is highly mode specific.

Dissipative IVR is observed at much lower energies in the complexes than in the bare molecule. A calculation of the density of vibrational states for the van der Waals modes can account for this observation when anharmonicities are included for the van der Waals modes.

We report five vibrational predissociation lifetimes from unknown, redistributed levels of the excited complex. In each case, the lifetime according to simple momentum gap law calculations depends so strongly on the unknown, final translational energy of the fragments and the (unknown) level of chemical and van der Waals vibrational excitation in the intermediate state, that no conclusion on the validity of the momentum-gap law can be made. In two cases, different VP lifetimes were measured for different redistributed levels of a particular excitation. In each case the product formed more rapidly differed from the initial state by a smaller number of vibrational quanta, not a smaller energy gap.

Predissociation rates calculated according to RRK theory are off by orders of magnitude and should not be used[31] to predict rates. Statistical RRKM theory, of course, cannot account for mode selectivity, or for different VP rates to different product states from isoenergetic levels. Simple RRKM calculations do, however, account for the magnitude of the observed VP rates for the major channels of the dissociation for stilbene–He_2 25[1], stilbene–Ne 25[1], and stilbene–Ar 25[3]. For other excitations where dissociation occurs, we observe no resolvable VP rates, which is also consistent with the calculated RRKM rates. We emphasize, however, that the calculation of RRKM rates for certain *vibrational predissociation* steps is only for comparison, since we observe non-RRKM behavior in that IVR is slow and mode selectivity prevails.

ACKNOWLEDGMENT

This work is supported by the National Science Foundation under Grant No. DMR-8521191.

[1] D. H. Semmes, J. S. Baskin, and A. H. Zewail, J. Am. Chem. Soc. **109**, 4104 (1987).
[2] J. A. Syage, P. M. Felker, and A. H. Zewail, J. Chem. Phys. **81**, 4685 (1984); J. A. Syage, W. R. Lambert, P. M. Felker, A. H. Zewail, and R. M. Hochstrasser, Chem. Phys. Lett. **88**, 268 (1982).
[3] (a) T. S. Zwier, E. Carrasquillo, M., and D. H. Levy, J. Chem. Phys. **78**, 5493 (1983); (b) C. A. Taatjes, W. B. Bosma, and T. S. Zwier, Chem. Phys. Lett. **128**, 127 (1986); (c) D. O. DeHaan, A. L. Holton, and T. S. Zwier, J. Chem. Phys. **90**, 3952 (1989).
[4] P. M. Felker, W. R. Lambert, and A. H. Zewail, J. Chem. Phys. **82**, 3003 (1985) and references therein.
[5] (a) J. S. Baskin and A. H. Zewail, J. Phys. Chem. **93**, 5701 (1989); (b) P. M. Felker and A. H. Zewail, J. Chem. Phys. **86**, 2460 (1987); (c) J. S. Baskin, P. M. Felker, and A. H. Zewail, *ibid.* **86**, 2483 (1987).
[6] T. Suzuki, N. Mikami, and M. Ito, J. Phys. Chem. **90**, 6431 (1986).
[7] L. H. Spangler, R. van Zee, and T. S. Zwier, J. Phys. Chem. **91**, 2782 (1987).
[8] (a) W. R. Lambert, P. M. Felker, and A. H. Zewail, J. Chem. Phys. **81**, 2217 (1984); (b) J. S. Baskin, P. M. Felker, and A. H. Zewail, *ibid.* **86**, 2483 (1987).
[9] (a) J. N. Demas, *Excited State Lifetime Measurements* (Academic, New York, 1983); (b) Desmond V. O'Connor and David Phillips, *Time-Correlated Single Photon Counting* (Academic, London, 1984); (c) P. R. Bevington, *Data Reduction and Error Analysis for the Physical Sciences* (McGraw–Hill, New York, 1969).
[10] J. A. Syage, P. M. Felker, and A. H. Zewail, J. Chem. Phys. **81**, 4706 (1984).
[11] (a) D. V. Brumbaugh, J. E. Kenny, and D. H. Levy, J. Chem. Phys. **78**, 3415 (1983); (b) K. W. Butz, D. L. Catlett, G. E. Ewing, D. Krajnovich, and C. S. Parmenter, J. Phys. Chem. **90**, 3533 (1986).
[12] A. Warshel, J. Chem. Phys. **62**, 214 (1975).
[13] T. Urano, M. Maegawa, K. Yamanouchi, and S. Tsuchiya, J. Phys. Chem. **93**, 3459 (1989).
[14] (a) A. Amirav and J. Jortner, Chem. Phys. Lett. **95**, 295 (1983); (b) T. J. Majors, U. Even, and J. Jortner, J. Chem. Phys. **81**, 2330 (1984).
[15] (a) W. M. van Herpen, Ph.D. thesis, Catholic University of Nijmegen, 1988; (b) D. Pratt (private communication).
[16] P. M. Felker, and A. H. Zewail, Chem. Phys. Lett. **108**, 303 (1984); Phys. Rev. Lett. **53**, 501 (1984); Adv. Chem. Phys. **70**, 265 (1988).
[17] F. Lahmani, A. Tramer, and C. Tric, J. Chem. Phys. **60**, 4431 (1974).
[18] U. Fano, Phys. Rev. **124**, 1866 (1961).
[19] S. W. Benson, *The Foundations of Chemical Kinetics* (McGraw–Hill, New York, 1960).
[20] G. E. Ewing, J. Phys. Chem. **90**, 1790 (1986).
[21] M. J. Ondrechen, Z. Berkovitch-Yellin, and J. Jortner, J. Am. Chem. Soc. **103**, 6586 (1981).
[22] M. M. Doxtader, I. M. Gulis, S. A. Schwartz, and M. R. Topp, Chem. Phys. Lett. **112**, 483 (1984); J. Wanna, and E. R. Bernstein, J. Chem. Phys. **84**, 927 (1986).
[23] I. I. Goldman and V. D. Krivchenkov, *Problems in Quantum Mechanics* (Pergamon, London, 1961).
[24] L. R. Khundkar, R. A. Marcus, and A. H. Zewail, J. Phys. Chem. **87**, 2473 (1983).
[25] G. E. Ewing, J. Chem. Phys. **72**, 2096 (1980).
[26] (a) D. F. Kelley and E. R. Bernstein, J. Phys. Chem. **90**, 5164 (1986); (b) L. R. Khundkar, J. L. Knee, and A. H. Zewail, J. Chem. Phys. **87**, 77 (1987).
[27] T. S. Zwier, J. Chem. Phys. **90**, 3967 (1989).
[28] W. R. Gentry, in *NATO Advanced Research Workshop on Structure and Dynamics of Weakly Bound Molecular Complexes*, edited by A. Weber (Reidel, Dordrecht, 1986), p. 467.
[29] (a) A. H. Zewail, Acc. Chem. Res. **13**, 360 (1980); (b) Ber. Bunsenges. Phys. Chem. **89**, 264 (1985).
[30] P. M. Weber and S. A. Rice, J. Phys. Chem. **92**, 5470 (1988).
[31] R. E. Smalley, J. Phys. Chem. **96**, 3504 (1982).